THE JOURNAL OF BIOLOGICAL CHEMISTRY
Vol. 279, No. 49, Issue of December 3, pp. 51376–51385, 2004
Printed in U.S.A.

Physical and Functional Interaction between Dorfin and Valosin-containing Protein That Are Colocalized in Ubiquitylated Inclusions in Neurodegenerative Disorders*

Received for publication, June 15, 2004, and in revised form, August 31, 2004
Published, JBC Papers in Press, September 29, 2004, DOI 10.1074/jbc.M406683200

Shinsuke Ishigaki‡§¶, Nozomi Hishikawa‡, Jun-ichi Niwa‡, Shun-ichiro Iemura‖, Tohru Natsume‖, Seiji Hori, Akira Kakizuka**‡‡, Keiji Tanaka§, and Gen Sobue‡§§**

*From the ‡Department of Neurology, Nagoya University Graduate School of Medicine, Nagoya 466-8500, Japan, the §Department of Molecular Oncology, Tokyo Metropolitan Institute of Medical Science, Tokyo 113-8613, Japan, the ‖National Institute of Advanced Science and Technology, Biological Information Research Center, Tokyo 135-0064, Japan, the **Laboratory of Functional Biology, Kyoto University Graduate School of Biostudies, Kyoto 606-8502, Japan, and ‡‡CREST, Japan Science and Technology Agency, Kawaguchi 332-0012, Japan*

Dorfin, a RING-IBR type ubiquitin ligase (E3), can ubiquitylate mutant superoxide dismutase 1, the causative gene of familial amyotrophic lateral sclerosis (ALS). Dorfin is located in ubiquitylated inclusions (UBIs) in various neurodegenerative disorders, such as ALS and Parkinson's disease (PD). Here we report that Valosin-containing protein (VCP) directly binds to Dorfin and that VCP ATPase activity profoundly contributes to the E3 activity of Dorfin. High through-put analysis using mass spectrometry identified VCP as a candidate of Dorfin-associated protein. Glycerol gradient centrifugation analysis showed that endogenous Dorfin consisted of a 400–600-kDa complex and was co-immunoprecipitated with endogenous VCP. *In vitro* experiments showed that Dorfin interacted directly with VCP through its C-terminal region. These two proteins were colocalized in aggresomes in HEK293 cells and UBIs in the affected neurons of ALS and PD. VCP^{K524A}, a dominant negative form of VCP, reduced the E3 activity of Dorfin against mutant superoxide dismutase 1, whereas it had no effect on the autoubiquitylation of Parkin. Our results indicate that VCPs functionally regulate Dorfin through direct interaction and that their functional interplay may be related to the process of UBI formation in neurodegenerative disorders, such as ALS or PD.

Amyotrophic lateral sclerosis (ALS)[1] is one of the most common neurodegenerative disorders, characterized by selective motor neuron degeneration in the spinal cord, brain stem, and cortex. Two genes, CuZn-superoxide dismutase (SOD1) and amyotrophic lateral sclerosis 2 have been identified as responsible genes for familial forms of ALS. Using mutant SOD1 transgenic mice, the pathogenesis of ALS has been partially uncovered. The proposed mechanisms of the motor neuron degeneration in ALS include oxidative toxicity, glutamate receptor abnormality, ubiquitin proteasome dysfunction, inflammatory and cytokine activation, dysfunction of neurotrophic factors, damage to mitochondria, cytoskeletal abnormalities, and activation of the apoptosis pathway (1, 2).

In a previous study (3), we identified several ALS-associated genes using molecular indexing. Dorfin was identified as one of the up-regulated genes in ALS, which contains a RING-IBR (in between ring finger) domain at its N terminus and mediated ubiquitin ligase (E3) activity (3, 4). Dorfin colocalized with Vimentin at the centrosome after treatment with a proteasome inhibitor in cultured cells (4). Dorfin physically bound and ubiquitylated various SOD1 mutants derived from familial ALS patients and enhanced their degradation, but it had no effect on the stability of wild-type SOD1 (5). Overexpression of Dorfin protected neural cells against the toxic effects of mutant SOD1 and reduced SOD1 inclusions (5).

Recent findings indicate that the ubiquitin-proteasome system is widely involved in the pathogenesis of Parkinson's disease (PD), Alzheimer's disease, polyglutamine disease, and Prion diseases as well as ALS (6). From this point of view, we previously analyzed the pathological features of Dorfin in various neurodegenerative diseases and found that Dorfin was predominantly localized not only in Lewy body (LB)-like inclusions in ALS but also in LBs in PD, dementia with Lewy bodies, and glial cell inclusions in multiple system atrophy (7). These characteristic intracellular inclusions composed of aggregated, ubiquitylated proteins surrounded by disorganized filaments are the histopathological hallmark of aging-related neurodegenerative diseases (8).

A structure called aggresome by Johnston *et al.* (9) is formed when the cell capacity to degrade misfolded proteins is exceeded. The aggresome has been defined as a pericentriolar, membrane-free, cytoplasmic inclusion containing misfolded ubiquitylated protein ensheathed in a cage of intermediate filaments, such as Vimentin (9). The formation of the aggresome mimics that of ubiquitylated inclusions (UBIs) in the affected neurons of various neurodegenerative diseases (10). Combined with the fact that Dorfin was localized in aggresomes in cultured cells and UBIs in ALS and other neurode-

* This work was supported by a grant for a Center of Excellence from the Ministry of Education, Culture, Sports, Science, and Technology of Japan. The costs of publication of this article were defrayed in part by the payment of page charges. This article must therefore be hereby marked "*advertisement*" in accordance with 18 U.S.C. Section 1734 solely to indicate this fact.

¶ Research resident of the Japan Foundation for Aging and Health, Psychiatric and Neurological Diseases, and Mental Health.

§§ To whom correspondence should be addressed: Dept. of Neurology, Nagoya University Graduate School of Medicine, Nagoya 466-8500, Japan. Tel.: 81-52-744-2385; Fax: 81-52-744-2384; E-mail: sobueg@med.nagoya-u.ac.jp.

[1] The abbreviations used are: ALS, amyotrophic lateral sclerosis; E3, ubiquitin ligase; ERAD, endoplasmic reticulum-associated degradation; LB, Lewy body; MS, mass spectrometry; LC-MS/MS, liquid chromatography coupled to electrospray tandem mass spectrometry; PD, Parkinson's disease; SOD1, CuZn-superoxide dismutase; UBI, ubiquitylated inclusions; VCP, valosin-containing protein; FLAG-Parkin, pcDNA3.1/FLAG-Parkin; Ub, ubiquitin; MBP, maltose-binding protein; GST, glutathione *S*-transferase; PBS, phosphate-buffered saline; HA, hemagglutinin; WT, wild type.

generative diseases, these observations suggest that Dorfin may have a significant role in the quality control system in the cell. The present study was designed to obtain further clues for the pathophysiological roles of Dorfin. For this purpose, we screened Dorfin-associated proteins using high performance liquid chromatography coupled to electrospray tandem mass spectrometry (LC-MS/MS). The results showed that Valosin-containing protein (VCP), also called p97 or Cdc48 homologue, obtained from the screening, physically and functionally interacted with Dorfin. Furthermore, both Dorfin and VCP proteins colocalized in aggresomes of the cultured cells and in UBIs in various neurodegenerative diseases.

MATERIALS AND METHODS

Plasmids and Antibodies—pCMV2/FLAG-Dorfin vector (FLAG-Dorfin^{WT}) was prepared by PCR using the appropriate design of PCR primers with restriction sites (ClaI and KpnI). The PCR product was digested and inserted into the ClaI-KpnI site in pCMV2 vector (Sigma). pEGFP-Dorfin (GFP-Dorfin), pCMX-VCP^{Wt} (VCP^{Wt}), and pCMX-VCP^{K524A} (VCP^{K524A}) vectors were described previously (5, 11). pcDNA/HA-VCP^{Wt} (HA-VCP^{Wt}) and pcDNA/HA-VCP^{K524A} (HA-VCP^{K524A}) were subcloned from pCMX-VCP^{Wt} and pCMX-VCP^{K524A}, respectively, into pcDNA3.1 vectors (Invitrogen). The HA tag was introduced at the N terminus of VCP. pcDNA3.1/FLAG-Parkin (FLAG-Parkin) was generated by PCR using the appropriate design of PCR primers with restriction sites (EcoRI and NotI) from pcDNA3.1/Myc-Parkin (12). The FLAG tag was introduced at the N terminus of Parkin. To establish the RING mutant plasmid of Dorfin (FLAG-Dorfin$^{C132S/C135S}$), point mutations for Cys at positions 132 and 135 to Ser were generated by PCR-based site-directed mutagenesis using a QuikChange™ site-directed mutagenesis kit (Stratagene, La Jolla, CA). pcDNA3.1/HA-Ub (HA-Ub), pcDNA3.1/Myc-SOD1^{WT} (SOD1^{WT}-Myc), pcDNA3.1/Myc-SOD1^{G93A} (SOD1^{G93A}-Myc), and pcDNA3.1/Myc-SOD1^{G85R} (SOD1^{G85R}-Myc) were described previously (13, 14). Polyclonal anti-Dorfin (Dorfin-30 and Dorfin-41) and monoclonal anti-VCP antibodies were used as in previous reports (5, 15). The following antibodies were used in this study: monoclonal anti-FLAG antibody (M2; Sigma), monoclonal anti-Myc antibody (9E10; Santa Cruz Biotechnology, Santa Cruz, CA), monoclonal anti-HA antibody (12CA5; Roche Applied Science), polyclonal anti-maltose-binding protein (MBP) antibody (New England BioLabs, Beverly, MA), polyclonal anti-Parkin (Cell Signaling, Beverly, MA), and polyclonal anti-SOD1 (SOD-100; Stressgen, San Diego, CA).

Cell Culture and Transfection—All media and reagents for cell culture were purchased from Invitrogen. HEK293 cells were grown in Dulbecco's modified Eagle's medium containing 10% fetal calf serum, 5 units/ml penicillin, and 50 μg/ml streptomycin. HEK293 cells at subconfluence were transfected with the indicated plasmids using FuGENE6 reagent (Roche Applied Science). To inhibit cellular proteasome activity, cells were treated with 1 μM MG132 (benzyloxycarbonyl-Leu-Leu-Leu-al; Sigma) for 16 h after overnight post-transfection. Cells were analyzed at 24–48 h after transfection.

Protein Identification by LC-MS/MS Analysis—FLAG-Dorfin^{WT} was expressed in HEK293 cells (semiconfluent in a 10-cm dish) and then immunoprecipitated by anti-FLAG antibody. The immunoprecipitates were eluted with a FLAG peptide and then digested with Lys-C endopeptidase (*Achromobacter* protease I). The resulting peptides were analyzed using a nanoscale LC-MS/MS system as described previously (16). The peptide mixture was applied to a Mightysil-PR-18 (1-μm particle, Kanto Chemical Corp., Tokyo) column (45 × 0.150 mm ID) and separated using a 0–40% gradient of acetonitrile containing 0.1% formic acid over 30 min at a flow rate of 50 nl/min. Eluted peptides were sprayed directly into a quadrupole time-of-flight hybrid mass spectrometer (Q-Tof *Ultima*; Micromass, Manchester, UK). MS and MS/MS spectra were obtained in data-dependent mode. Up to four precursor ions above an intensity threshold of 10 cps were selected for MS/MS analysis from each survey scan. All MS/MS spectra were searched against protein sequences of Swiss Prot and RefSeq (NCBI) using batch processes of the Mascot software package (Matrix Science, London, UK). The criteria for match acceptance were the following: 1) when the match score was 10 over each threshold, identification was accepted without further consideration; 2) when the difference of score and threshold was lower than 10 or when proteins were identified based on a single matched MS/MS spectrum, we manually confirmed the raw data prior to acceptance; 3) peptides assigned by less than three y series ions and peptides with +4 charge state were all eliminated regardless of their scores.

Recombinant Proteins and Pull-down Assay—We used pMALp2 (New England BioLabs) and pMALp2T (Factor Xa cleavage site of pMALp2 was replaced with a thrombin recognition site) to express fusion proteins with MBP. To produce the full-length (residues 1–838) Dorfin (MBP-Dorfin^{full}), N-terminal (residues 1–367) Dorfin (MBP-Dorfin^{N}), and C-terminal (residues 368–838) Dorfin (MBP-Dorfin^{C}), the PCR fragments were amplified from pcDNA4/HisMax-Dorfin (4) by using the appropriate PCR primers with restriction sites (FbaI and HindIII) and then ligated into pMAL-p2 vectors. To produce the MBP-Parkin protein, full-length *PARKIN* cDNA was inserted into the EcoRI-NotI sites of pMALp2T. All of the MBP-tagged recombinant proteins were purified from *Escherichia coli* BL21-codon-plus. The detail of the purification method of MBP-tagged proteins was described previously (17). Recombinant GST fusion VCP^{WT} and VCP^{K524A} proteins were also generated from *E. coli* lysate and purified with glutathione-Sepharose. Recombinant His-VCP^{WT} and His-VCP^{K524A} proteins were purified from insect cells using baculovirus. The detail of purification of these recombinant VCP proteins was described previously (15). Binding experiments were performed with proteins carrying different tags. His- or GST-VCP were mixed with MBP fusion proteins: MBP-Dorfin^{full}, -Dorfin^{N}, -Dorfin^{C}, -Parkin, and -mock. His-VCP and GST-VCP proteins were precipitated by Ni^{2+}-nitrilotriacetic acid-agarose (Qiagen, Valencia, CA), and glutathione-Sepharose (Amersham Biosciences), respectively. Binding was performed with 1–3 μg of each protein in 300 μl of binding buffer (50 mM Tris-HCl, pH 7.5, 100 mM NaCl, 5 mM $MgCl_2$, 10% glycerol, 0.5 mg/ml bovine serum albumin, 1 mM dithiothreitol) for 1 h at 4 °C. Then 15 μl of beads were added and incubated for 30 min. The beads were washed by binding buffer three times and eluted with sample buffer and analyzed by SDS-PAGE followed by Western blotting using specific antibodies.

Glycerol Gradient Centrifugation—Cultured cells or mouse tissues were homogenized in 1 ml of PBS with protease inhibitor (Complete Mini; Roche Applied Science). Supernatants (1 mg of protein for cultured cells, 5 mg of protein for mouse tissues, and 0.1 mg of recombinant His-VCP protein) were used as the samples after 10,000 × *g* centrifugation for 20 min. The samples (1.0 ml) were loaded on top of a 34-ml linear gradient of glycerol (10–40%) prepared in 25 mM Tris-HCl buffer, pH 7.5, containing 1 mM dithiothreitol in 40 PA centrifuge tubes (Hitachi, Tokyo), and centrifuged at 4 °C and 80,000 × *g* for 22 h using a Himac CP100α centrifuge system (Hitachi). Thirty fractions were collected from the top of the tubes. Two hundred μl of each fraction was precipitated with acetone, and the remaining pellet was lysed with 50 μl of sample buffer and then used for SDS-PAGE followed by Western blotting.

Immunological Analysis—Cells (4 × 10^5 in a 6-cm dish) were lysed with 500 μl of lysis buffer (50 mM Tris-HCl, 150 mM NaCl, 1% Nonidet P-40, and 1 mM EDTA) with protease inhibitor mixture (Complete Mini) 24–48 h after transfection. The lysate was then centrifuged at 10,000 × *g* for 10 min at 4 °C to remove debris. A 10% volume of the supernatants was used as the "lysate" for SDS-PAGE. When immunoprecipitated, the supernatants were precleared with protein A-Sepharose (Amersham Biosciences), and specific antibodies, anti-FLAG (M2), anti-Myc (9E10), or anti-Dorfin (Dorfin-30) were then added and then incubated at 4 °C with rotation. Immune complexes were then incubated with protein A-Sepharose for 3 h, collected by centrifugation, and washed four times with the lysis buffer. For protein analysis, immune complexes were dissociated by heating in SDS-PAGE sample buffer and loaded onto SDS-PAGE. The samples were separated by SDS-PAGE (12% gel or 4–12% gradient gel) and transferred onto a polyvinylidene difluoride membrane. Finally, Western blotting was performed with specific antibodies.

Immunohistochemistry—HEK293 cells grown on glass coverslips were fixed in 4% paraformaldehyde in PBS for 15 min. Then the cells were blocked for 30 min with 5% (v/v) normal goat serum in PBS, incubated for 1 h at 37 °C with anti-HA antibody (12CA5), washed with PBS, and incubated for 30 min with Alexa 496-nm anti-mouse antibodies (Molecular Probes, Inc., Eugene, OR). The coverslips were washed and mounted on slides. Fluorescence images were obtained using a fluorescence microscope (DMIRE2; Leica, Bannockburn, IL) equipped with a cooled charge-coupled device camera (CTR MIC; Leica). Pictures were taken using Leica Qfluoro software.

Pathological Studies—Pathological studies were carried out on 10% formalin-fixed, paraffin-embedded spinal cords and brain stems filed in the Department of Neurology, Nagoya University Graduate School of Medicine. The specimens were obtained at autopsy from three sporadic cases of ALS and four sporadic PD patients. The spinal cord and brain stem specimens of these ALS and PD cases were immunohistochemically stained with antibodies against Dorfin (Dorfin-41) and VCP. Dou-

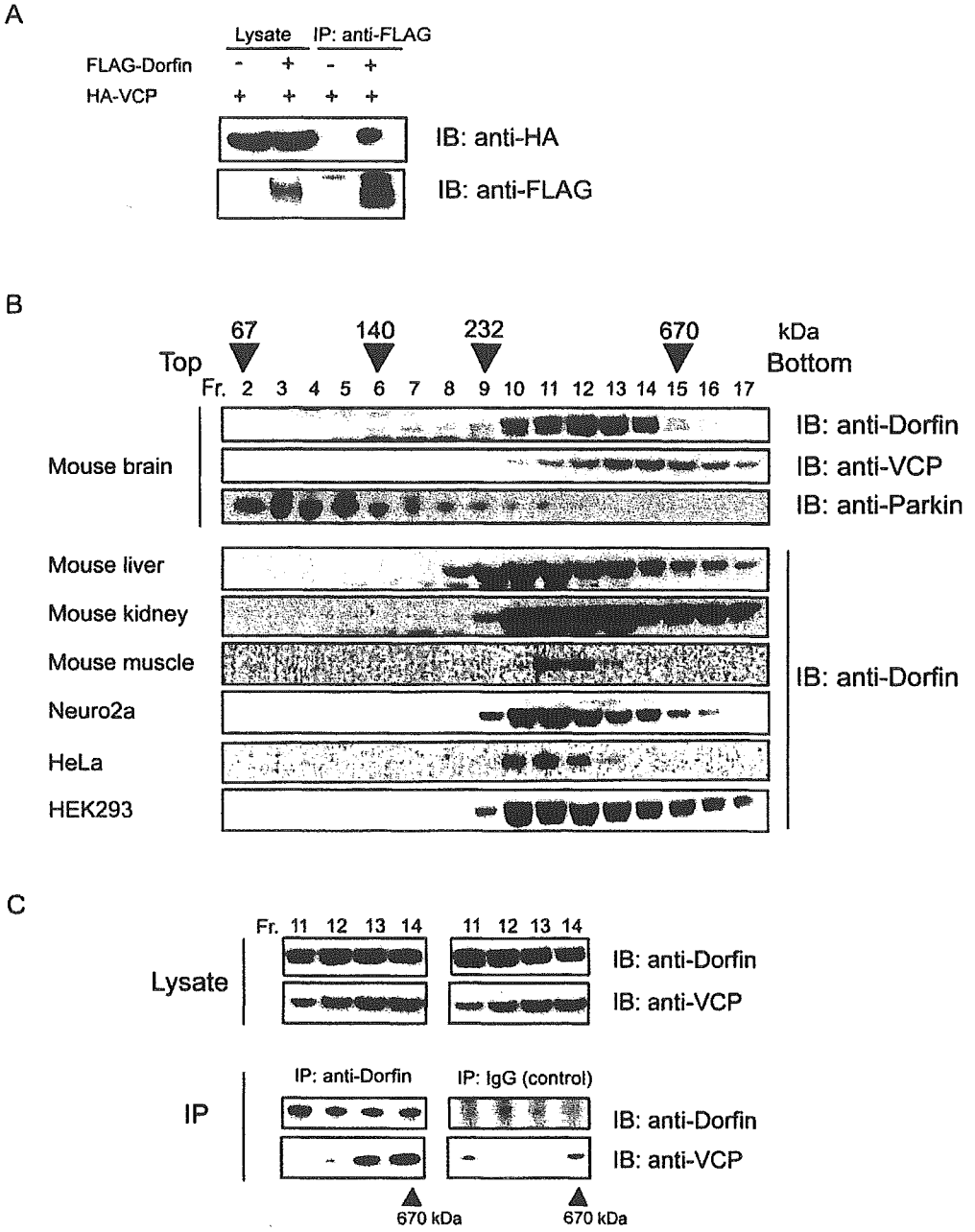

FIG. 1. ***In vivo* interaction between Dorfin and VCP.** *A*, FLAG-Dorfin and HA-VCP are co-expressed in HEK293 cells. FLAG-mock vector was used as a negative control. The amounts of HA-VCP in 10% of the lysate used are shown (*Lysate*); the rest was subjected to immunoprecipitation (*IP*) with anti-FLAG (M2) antibody. Following immunoblotting (*IB*) with anti-HA (12CA5) antibody revealed that HA-VCP was co-immunoprecipitated with FLAG-Dorfin. *B*, 5 mg of protein of various mouse tissues (brain, liver, kidney, and muscle) and 1 mg of protein of cultured cells (HEK293, HeLa, and Neuro2a) were each homogenized in 1 ml of PBS. Supernatants were fractionated by 10–40% glycerol gradient centrifugation followed by separation into 30 fractions using a fraction collector. Immunoblotting using anti-Dorfin, anti-VCP, and anti-Parkin antibodies was performed on the fractions (*Fr.*), including fractions 2–17. Endogenous Dorfin was co-sedimented with VCP in the fractions with a molecular mass of around 400–600 kDa. The positions of co-migrated molecular mass markers are indicated *above* the *panels*. *C*, immunoprecipitation with polyclonal anti-Dorfin antibody (anti-Dorfin-30) was performed on fractions 11–14 collected by glycerol gradient centrifugation analysis, where endogenous Dorfin was seen in *B*. As a negative control, immunoprecipitation with nonimmune rabbit IgG was used on the same fractions.

ble staining of identical sections was performed as described previously (7). In immunofluorescence microscopy, Alexa-488- and Alexa-546-conjugated secondary antibodies (Molecular Probes) were used. All human and animal studies described in this report were approved by the appropriate Ethics Review Committees of the Nagoya University Graduate School of Medicine.

RESULTS

Identification of Dorfin-associated Protein in the Cells—In an effort to identify protein(s) that physically interacts with Dorfin in the cells, FLAG-Dorfin was expressed in HEK293 cells and then immunoprecipitated by anti-FLAG antibody. The immunoprecipitates were eluted with a FLAG peptide and then digested with Lys-C endopeptidase (*Achromobacter* protease I), and the cleaved fragments were directly analyzed using a highly sensitive "direct nanoflow LC-MS/MS" system as described under "Materials and Methods." Following data base search, a total of 13 peptides were assigned to MS/MS spectra obtained from the LC-MS/MS analyses for the FLAG-Dorfin-

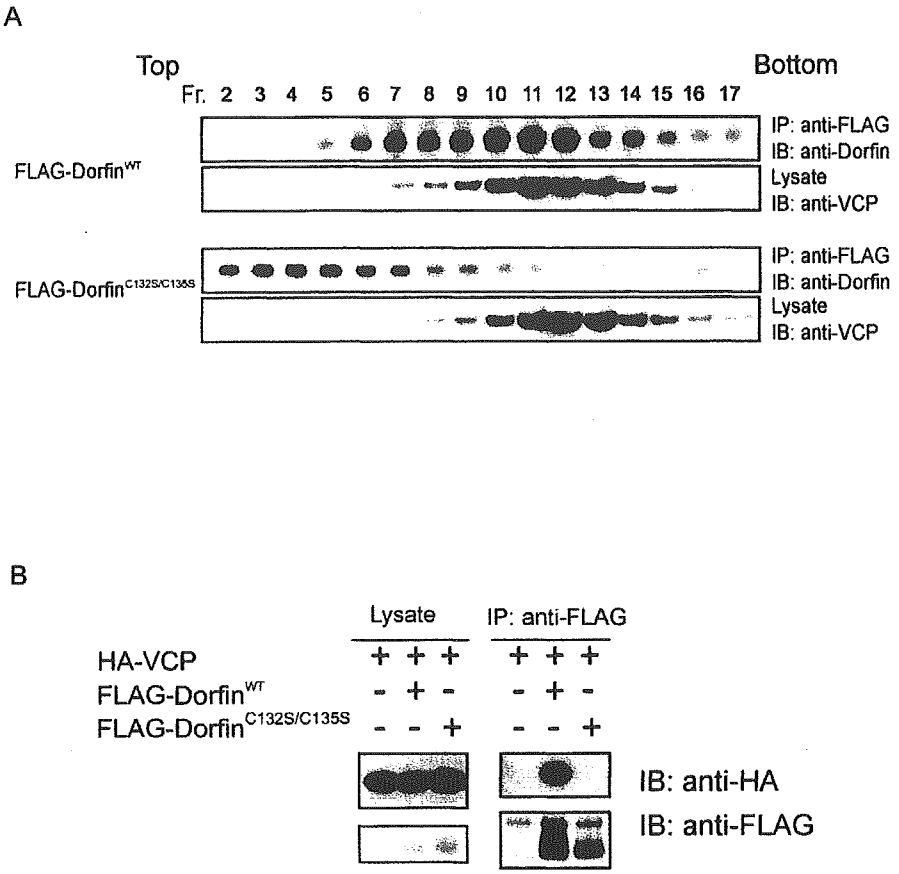

FIG. 2. **Loss of physical interaction between Dorfin$^{C132S/C135S}$ and VCP.** *A*, transfected Dorfin^{WT}, but not Dorfin$^{C132S/C135S}$ (*Dorfin$^{C132S-C135S}$*), forms a high M_r complex. Lysate of HEK293 cells overexpressed with FLAG-Dorfin^{WT} or FLAG-Dorfin$^{C132S/C135S}$ was fractionated by 10–40% glycerol gradient centrifugation. The selected fractions (*Fr.*), fractions 2–17, were subjected to immunoprecipitation (*IP*) using anti-FLAG (M2) antibody. Immunoblotting (*IB*) with anti-Dorfin antibody revealed that exogenous FLAG-Dorfin^{WT} formed a high molecular weight complex, whose peak was at fraction 11, whereas FLAG-Dorfin$^{C132S/C135S}$ migrated in fractions of smaller M_r (around fraction 7). Ten percent of the fractionated samples were shown as "lysate." *B*, Dorfin^{WT} can interact with VCP, but Dorfin$^{C132S/C135S}$ cannot. FLAG-Dorfin^{WT} or FLAG-Dorfin$^{C132S/C135S}$ and HA-VCP were co-expressed in HEK293 cells. FLAG-mock vector was used as a negative control. The amounts of HA-VCP in 10% of the lysate used are shown (*Lysate*); the rest was subjected to immunoprecipitation with anti-FLAG (M2) antibody. Following immunoblotting with anti-HA (12CA5) antibody revealed that HA-VCP was co-immunoprecipitated with FLAG-Dorfin^{WT} but not with FLAG-Dorfin$^{C132S/C135S}$.

associated complexes. These peptide data identified nine proteins as candidates for Dorfin-associated proteins. One of these identified proteins was VCP that has been proposed to have multiple functions, such as membrane fusion or endoplasmic reticulum-associated degradation (ERAD) (18–22). In the next step, we examined the relationship between Dorfin and VCP, because the latter has been reported to be linked to various aspects of neurodegeneration (15).

Dorfin Interacts with VCP in Vivo—To verify the interaction between Dorfin and VCP, FLAG-Dorfin and HA-VCP were transiently overexpressed in HEK 293 cells. Immunological analyses revealed that HA-VCP was co-immunoprecipitated with FLAG-Dorfin but not with FLAG-mock (Fig. 1*A*), confirming their physical interactions in the cells. To determine whether endogenous Dorfin forms a complex, the lysate from mouse brain homogenate was fractioned by glycerol density gradient centrifugation. Each fraction was immunoblotted with anti-Dorfin antibody. The majority of endogenous Dorfin was co-sedimented with VCP around a size of 400–600 kDa, although endogenous Parkin, which is another RING-IBR type E3 ligase (12), existed in the fractions of much lighter molecular weight (M_r) (Fig. 1*B*, *top panels*). Moreover, Dorfin was sedimented in the fractions of 400–600 kDa in other tissues, such as the liver, kidney, and muscle of mouse, and various cultured cells including Neuro2a, HeLa, and HEK293 cells (Fig. 1*B*, *bottom panels*). To determine whether endogenous Dorfin interacts with VCP, immunoprecipitation using polyclonal anti-Dorfin antibody (Dorfin-30) was performed on the fractions shown in Fig. 1*B*, *top panels*. Endogenous VCP was co-immunoprecipitated with endogenous Dorfin in the fractions of high M_r (fractions (*Fr.*) 13 and 14). No apparent band was observed when precipitated with rabbit IgG (Fig. 1*C*).

Mutations of RING Finger Domain of Dorfin Results in Loss of Dorfin-VCP Interactions—Next, we examined whether transfected Dorfin (FLAG-Dorfin^{WT}) and its RING mutant (FLAG-Dorfin$^{C132S/C135S}$), in which the two Cys residues at positions 132 and 135 within the RING finger domain were substituted for Ser residues, form a complex. The results showed overexpression of FLAG-Dorfin^{WT} in high molecular fractions (*Fr.* in Fig. 2), whose peak was between fractions 10 and 12, whereas overexpressed FLAG-Dorfin$^{C132S/C135S}$ did not consist of high molecular weight complex. Overexpression of FLAG-Dorfin^{WT} or FLAG-Dorfin$^{C132S/C135S}$ did not change the sedimentation pattern of VCP (Fig. 2*A*). Furthermore, immunoprecipitation analysis showed that FLAG-Dorfin^{WT}, but not FLAG-Dorfin$^{C132S/C135S}$, could interact with HA-VCP in HEK293 cells (Fig. 2*B*).

Dorfin Interacts with VCP in Vitro—To confirm the direct

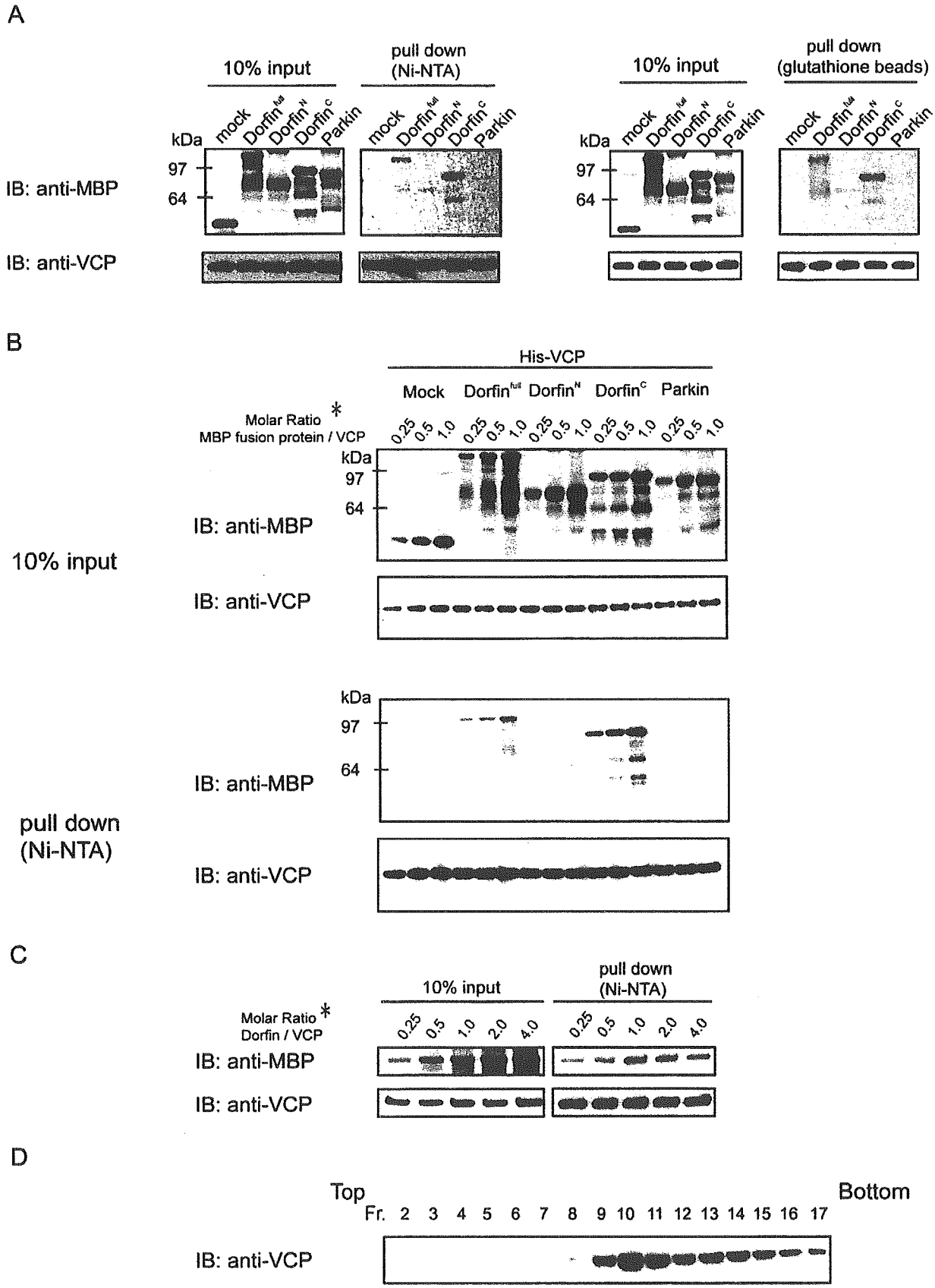

FIG. 3. ***In vitro* interaction between Dorfin and VCP.** *A*, recombinant His- or GST-VCP protein was incubated with MBP-mock, MBP-Dorfin^{full}, MBP-Dorfin^{N}, MBP-Dorfin^{C}, and MBP-Parkin proteins *in vitro*. Two μg of His- or GST-VCP proteins and MBP fusion proteins at similar molar concentrations to VCP proteins were used for the assays. The amounts of MBP fusion and GST fusion Dorfin derivatives and His-VCP in 10% of the samples used are shown (*10% input*). *NTA*, nitrilotriacetic acid. *IB*, immunoblot. *B*, 2 μg of His-VCP was incubated with MBP-mock,

binding between Dorfin and VCP and to determine the exact portion of Dorfin that interacts with VCP *in vitro*, we performed pull-down assays using recombinant proteins. Recombinant MBP-Dorfin or its deletion mutants (*i.e.* MBP-Dorfin^{N} and MBP-Dorfin^{C}) and the same molar of recombinant His-VCP or GST-VCP were mixed and incubated for 1 h at 4 °C. MBP-mock protein was used as a negative control in these experiments. A small portion of MBP-Dorfin^{full} or Dorfin^{C} (C-terminal substrate-recognizing domain) bound to both His-VCP and GST-VCP, whereas MBP-mock, MBP-Dorfin^{N} (N-terminal RING-IBR domain), and MBP-Parkin did not bind to His-VCP or GST-VCP (Fig. 3*A*). We next determined the number of Dorfins that bind one hexamer of VCP. To investigate this issue, we incubated His-VCP with increasing amounts of MBP-Dorfin^{full}, MBP-Dorfin^{N}, MBP-Dorfin^{C}, MBP-mock, or MBP-Parkin. As shown in Fig. 3*B*, the amount of binding portion of MBP-Dorfin^{full} and -Dorfin^{C} pulled down with His-VCP was not saturated below the even molar ratio. The pull-down experiments using excess amounts of MBP-Dorfin^{full} revealed that MBP-Dorfin^{full} was saturated at the even molar ratio (Fig. 3*C*). As reported previously (15), recombinant His-VCP sedimented in high molecular weight fractions, indicating that it formed a hexamer *in vitro* (Fig. 3*D*). These findings indicated that six Dorfin molecules were likely bind to a VCP complex *in vitro*.

Subcellular Localization of Dorfin and VCP in HEK293 Cells—In previous studies, we showed that exogenous and endogenous Dorfin resided perinuclearly and was colocalized with Vimentin in cultured cells treated with a proteasome inhibitor (4). The staining patterns of Dorfin were indistinguishable from those of the aggresome, namely a pericentriolar, membrane-free, cytoplasmic inclusion containing misfolded ubiquitylated proteins packed in a cage of intermediate filaments (4). VCP immunostaining was also observed throughout aggresomes in cultured neuronal cells when induced by treatment with a proteasome inhibitor (15). In order to examine the subcellular localization of Dorfin and VCP, GFP-Dorfin and HA-VCP were co-expressed in HEK293 cells. Without proteasome treatment, GFP-Dorfin-expressing cells showed granular fluorescence in the cytosol, and the HA-VCP-expressing cells showed diffuse and uniform cytoplasmic staining (Fig. 4*A*). Treatment with MG132 (1 μM, 16 h) resulted in accumulation of both GFP-Dorfin and HA-VCP and perinuclear colocalization as a clear large protein aggregate that mimics aggresomes (Fig. 4*B*).

Colocalization of Dorfin and VCP in the Affected Neurons of ALS and PD—In previous studies, immunostaining of Dorfin and VCP was independently noted in LBs of PD, and the peripheral staining pattern of both proteins in LBs was similar (7, 23). To confirm the immunoreactivities of Dorfin and VCP in the affected neurons in ALS and PD, we performed a double-labeling immunofluorescence study using a rabbit polyclonal anti-Dorfin antibody (Dorfin-41) and a mouse monoclonal VCP antibody on the postmortem samples of ALS and PD. In the ALS spinal cords, both proteins were colocalized in the LB-like inclusions (Fig. 5, *A–F*). The margin of LBs in PD was intensely immunostained for Dorfin and VCP, and merged images confirmed their strong colocalization (Fig. 5, *G–L*). Dorfin and VCP were also positive in Lewy neurites in the affected neurons of PD (Fig. 5, *M–O*).

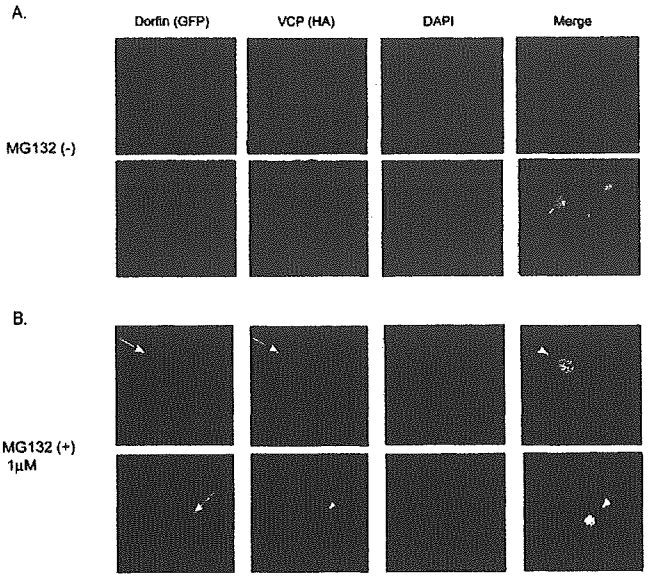

FIG. 4. **Subcellular localization of GFP-Dorfin and HA-VCP in HEK293 cells treated or untreated with a proteasome inhibitor.** GFP-Dorfin and HA-VCP were co-expressed transiently in HEK 293 cells. Cells were treated with (*B*) or without (*A*) 1 μM MG132 for 16 h. HA-VCP was stained with anti-monoclonal HA antibody (12CA5). Nuclei were stained with 4′,6-diamidino-2-phenylindole (*DAPI*). Without the treatment of MG132, GFP-Dorfin was spread through the cytosol, and it appeared like small aggregations. HA-VCP was also seen mainly in the cytosol and partly colocalized with GFP-Dorfin (*A*). After treatment with 1 μM MG132 for 16 h, both GFP-Dorfin and HA-VCP showed perinuclear accumulation and colocalization and appeared as clear large protein aggregates (*B*; *arrows*).

Dorfin Ubiquitylates Mutant SOD1 in Vivo—Unlike the wild-type form, mutant SOD1 proteins are rapidly degraded by the ubiquitin-proteasome system. Consistent with our previous results (5), SOD1^{G93A} and SOD1^{G85R} were polyubiquitylated, and co-expression with FLAG-Dorfin^{WT} enhanced polyubiquitylation of these mutant SOD1s compared with co-expression with FLAG-BAP, a negative control construct (Fig. 6*A*). Boiling with 1% SDS-containing buffer did not change the level of ubiquitylated mutant SOD1, indicating that mutant SOD1 itself was ubiquitylated by Dorfin (Fig. 6*B*). We also performed the same *in vivo* ubiquitylation assay using Neuro2a cells to examine for E3 activity of Dorfin in neuronal cells. The enhanced polyubiquitylation of these mutant SOD1s by Dorfin was observed in Neuro2a cells as well as in HEK293 cells (Fig. 6*C*). FLAG-Dorfin$^{C132S/C135S}$ did not enhance polyubiquitylation of mutant SOD1s, indicating that this RING finger mutant form was functionally inactive (Fig. 6*D*).

VCP^{K524A} Suppresses the E3 Activity of Dorfin—VCP has two ATPase binding domains (D1 and D2). A D2 domain mutant, VCP^{K524A}, induces cytoplasmic vacuoles, which mimics vacuole formation seen in the affected neurons in various neurodegenerative diseases (11, 15). The D2 domain represents the major ATPase activity and is essential for VCP function (11). The ATPase activity of VCP^{K524A} is much lower than that of VCP^{WT}, and VCP^{K524A} caused accumulation of polyubiquitylated proteins in the nuclear and membrane fractions together with elevation of ER stress marker proteins due to ERAD

MBP-Dorfin^{full}, MBP-Dorfin^{N}, MBP-Dorfin^{C}, and MBP-Parkin with increasing amounts (molar ratio to VCP: 0.25, 0.5, and 1.0). The amounts of MBP fusion Dorfin derivatives and His-VCP in 10% of the samples used are shown (10% input). *C*, 2 μg of His-VCP was incubated with MBP-Dorfin^{full} with increasing amounts (molar ratio to VCP: 0.25, 0.5, 1, 2, and 4). The amounts of MBP-Dorfin^{full} and His-VCP in 10% of the samples used are shown (*10% input*). *D*, His-VCP protein (0.5 μg) was fractionated by 10–40% glycerol gradient centrifugation followed by separation into 30 fractions using a fraction collector. Immunoblotting using anti-VCP antibody was performed on the selected fractions (fractions 2–17). *, The molar ratio was calculated by the amount of VCP monomers, not VCP complexes.

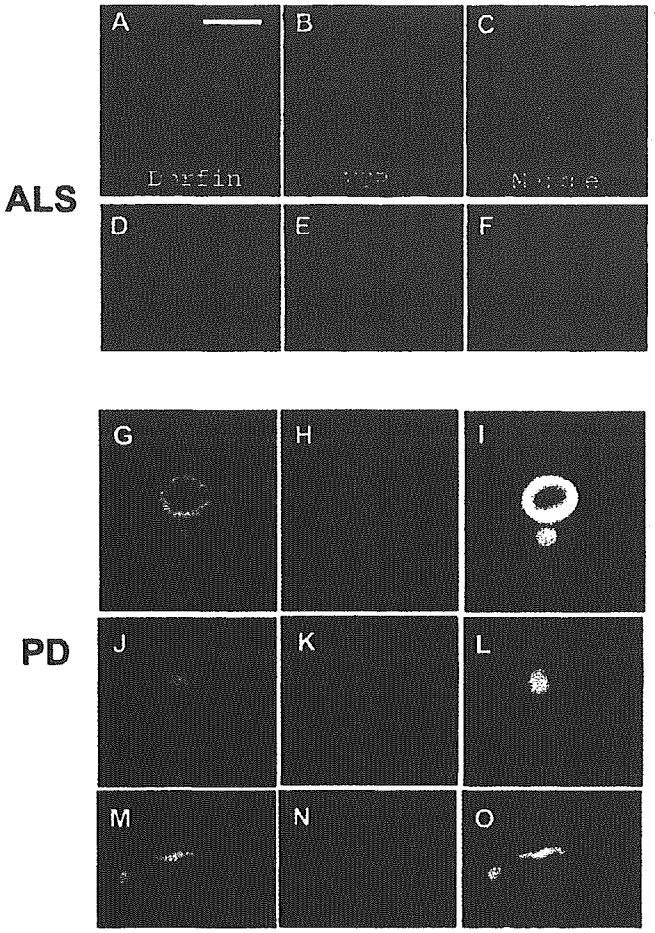

FIG. 5. **Colocalization of Dorfin-41 immunoreactivity with VCP in neuronal inclusions in ALS and PD.** Sections were doubly labeled with anti-Dorfin-41 antiserum and monoclonal VCP antibody and analyzed with a laser-scanning confocal microscope. The *left panels* (*green*) correspond to Dorfin, *middle panels* (*red*) correspond to VCP, and *right panels* correspond to merged images; structures in *yellow* indicate colocalization. Colocalization of Dorfin and VCP is seen in LB-like inclusions in motor neurons of the spinal cord of ALS (*A–F*). Dorfin is also colocalized with VCP in the margin of LBs (*G–I*), premature LBs (*J–L*), and Lewy neurites (*M–O*) in the nigral neurons of PD. *Scale bars*, 20 μm (*A–L*) and 10 μm (*M–O*).

inhibition, whereas its expression level, localization, and complex formation were indistinguishable from those of VCP^{WT} (11). In order to examine the functional effect of VCP on Dorfin, VCP^{WT}, VCP^{K524A}, or LacZ was co-expressed with $SOD1^{G85R}$, FLAG-Dorfin, and HA-Ub in HEK293 cells. Co-expression with VCP^{K524A} showed a marked decline of polyubiquitylation of $SOD1^{G85R}$ compared with co-expression with VCP^{WT} or LacZ (Fig. 7*A*, *top* and *middle*). Since Dorfin physically interacts with mutant SOD1s (5), we next investigated whether this decline of polyubiquitylation of $SOD1^{G85R}$ was mediated by reduced affinity between $SOD1^{G85R}$ and Dorfin. Immunoprecipitation by anti-FLAG antibody showed that VCP^{K524A} did not change affinity between $SOD1^{G85R}$ and Dorfin (Fig. 7*A*, *bottom*). Neither VCP^{WT} nor VCP^{K524A} changed the level of polyubiquitylation protein in the total lysate (Fig. 7*B*). To clarify whether this negative effect of VCP^{K524A} is specific for Dorfin, we assessed the autoubiquitylation of FLAG-Parkin in the presence of VCP^{WT}, VCP^{K524A}, or LacZ. Co-expression of VCP^{K524A} did not decrease autoubiquitylation of FLAG-Parkin compared with co-expression of LacZ or VCP^{WT} (Fig. 7*C*). We performed the same experiments using Neuro2a cells to see whether VCP^{K524A} suppress the E3 activity of Dorfin in neuronal cells. The marked decline of polyubiquitylation of $SOD1^{G85R}$ by VCP^{K524A} expression was also seen in Neuro2a cells (Fig. 7*D*).

DISCUSSION

UBIs in the affected neurons are histopathological hallmarks in various neurodegenerative disorders (8). Dorfin is an E3 ligase, which can ubiquitylate mutant SOD1s and synphilin-1 (5, 24). These substrates and Dorfin were identified in UBIs in various neurodegenerative diseases, such as LB-like inclusions in ALS and LBs in PD and dementia with Lewy bodies (7). This finding suggests that Dorfin may play a crucial role in the process of generating inclusions in the affected neurons. In the present study, we identified VCP as one of the Dorfin-associated proteins using mass spectrometry, and VCP-Dorfin physical interaction was confirmed by an immunoprecipitation experiment using FLAG-Dorfin and HA-VCP overexpressed in HEK293 cells (Fig. 1*A*). VCP is an essential and highly conserved protein of the AAA-ATPase family, which is considered to have diverse cellular functions, such as membrane fusion (25–27), nuclear trafficking (28), cell proliferation (29, 30), and the ERAD pathway (18–22). Many reports have implied that VCP is involved in the pathogenesis of various neuromuscular diseases. VCP has been implicated as a factor that modifies the progress of polyglutamine-induced neuronal cell death (15). In addition, histopathological studies revealed positive staining for VCP in UBIs in PD and ALS with dementia (23). VCP is also associated with MJD protein/atxin-3, in which abnormal expansion of polyglutamine tracts causes Machado-Joseph disease/spinocerebellar ataxia type 3 (31). VCP is also required for the degradation of ataxin-3 in collaboration with E4B/Ufd2a, a ubiquitin chain assembly factor (E4) (32). Recent studies have indicated that missense mutations in the VCP gene cause inclusion body myopathy associated with Paget's disease of bone and frontotemporal dementia, which is characterized by the presence of vacuoles in the cytoplasm in muscle fibers (33).

Our results showed that endogenous Dorfin formed a 400–600-kDa complex in various tissues and various cultured cells (Fig. 1*B*). Dorfin is a ~91-kDa protein; therefore, this high M_r complex should include Dorfin-associated proteins, although the possibility that Dorfin itself oligomerizes in the cell cannot be excluded. Glycerol gradient centrifugation analysis and immunoprecipitation experiments in the present study showed that endogenous Dorfin interacted with endogenous VCP in a complex of approximately 600 kDa, possibly including a Dorfin molecule and a hexametric form of VCP (Fig. 1*C*).

The first RING mutant of Dorfin, in which Cys at positions 132 and 135 changed to Ser, was prepared. This mutant Dorfin, $Dorfin^{C132S/C135S}$, could not ubiquitylate mutant SOD1s (Fig. 6*D*). Glycerol gradient centrifugation analysis revealed that $Dorfin^{C132S/C135S}$ did not form a high M_r complex, whereas exogenous wild type Dorfin ($Dorfin^{WT}$) formed a high M_r complex similar to endogenous Dorfin (Fig. 2*A*). Furthermore, an immunoprecipitation experiment using $Dorfin^{WT}$ and $Dorfin^{C132S/C135S}$ revealed that $Dorfin^{WT}$ could interact with VCP, whereas $Dorfin^{C132S/C135S}$ could not (Fig. 2*B*).

Our *in vitro* study using recombinant proteins showed that full-length ($MBP\text{-}Dorfin^{full}$) and the C terminus of Dorfin ($MBP\text{-}Dorfin^{C}$) directly interacted with VCP, whereas the $MBP\text{-}Dorfin^{N}$ mutant, containing the entire RING finger domain (amino acid residues 1–367), did not bind to VCP (Fig. 3*A*). This finding was unexpected, since *in vivo* binding analysis suggested that Dorfin could interact with VCP at the RING finger domain. It is plausible that certain structural changes in $Dorfin^{C132S/C135S}$ might render the C-terminal VCP-binding portion incapable of accessing VCP molecules. This may explain the result that $Dorfin^{C132S/C135S}$ did not form a high M_r complex.

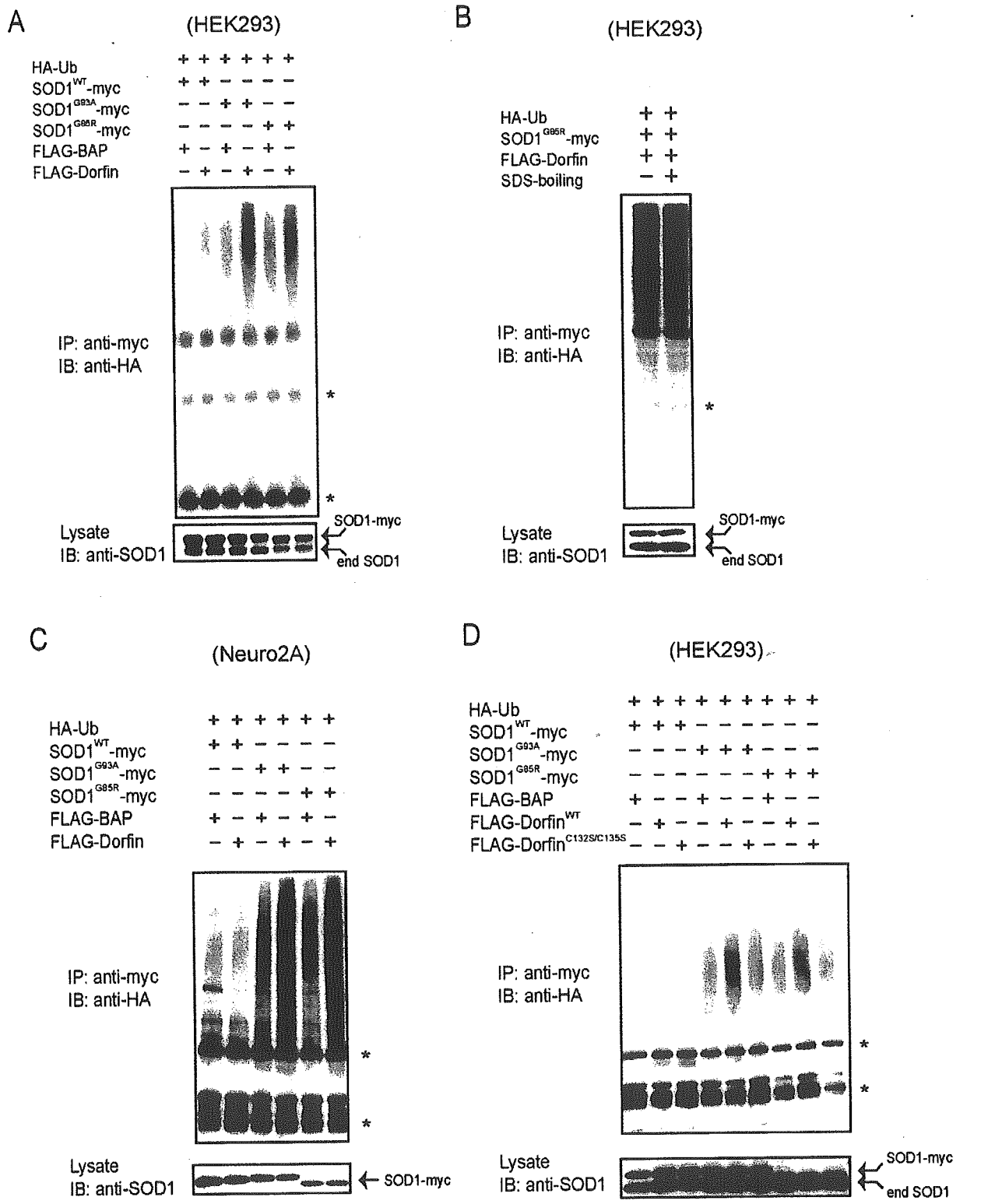

FIG. 6. **Dorfin ubiquitylates mutant SOD1s *in vivo*.** *A*, increased ubiquitylation of mutant SOD1 proteins by overexpression of Dorfin. HEK293 cells were co-transfected with $SOD1^{WT}$-Myc, $SOD1^{G93A}$-Myc, or $SOD1^{G85R}$-Myc and HA-Ub with or without FLAG-Dorfin. FLAG-bovine alkaline phosphatase (*BAP*) was used as a negative control. Immunoprecipitation (*IP*) was performed with Myc antibody (9E10). *IB*, immunoblotting. *B*, SDS boiling was performed prior to immunoprecipitation. To examine covalently ubiquitylated molecules, the cell lysate was boiled with the buffer containing 1% SDS for 5 min. Immunoprecipitation with Myc antibody (9E10) showed that the SDS-boiling procedure did not change polyubiquitylation level of $SOD1^{G85R}$-Myc by Dorfin. *C*, increased ubiquitylation of mutant SOD1 proteins by overexpression of Dorfin in Neuro2a cells. The same *in vivo* ubiquitylation assay as in *A* was performed using Neuro2a cells. *D*, $Dorfin^{C132S/C135S}$ ($Dorfin^{C132S/C135S}$) did not have E3 activity on mutant SOD1. HEK293 cells were co-transfected with $SOD1^{WT}$-Myc, $SOD1^{G93A}$-Myc, or $SOD1^{G85R}$-Myc and HA-Ub with FLAG-$Dorfin^{WT}$ or FLAG-$Dorfin^{C132S/C135S}$. The *asterisks* indicate IgG light and heavy chains.

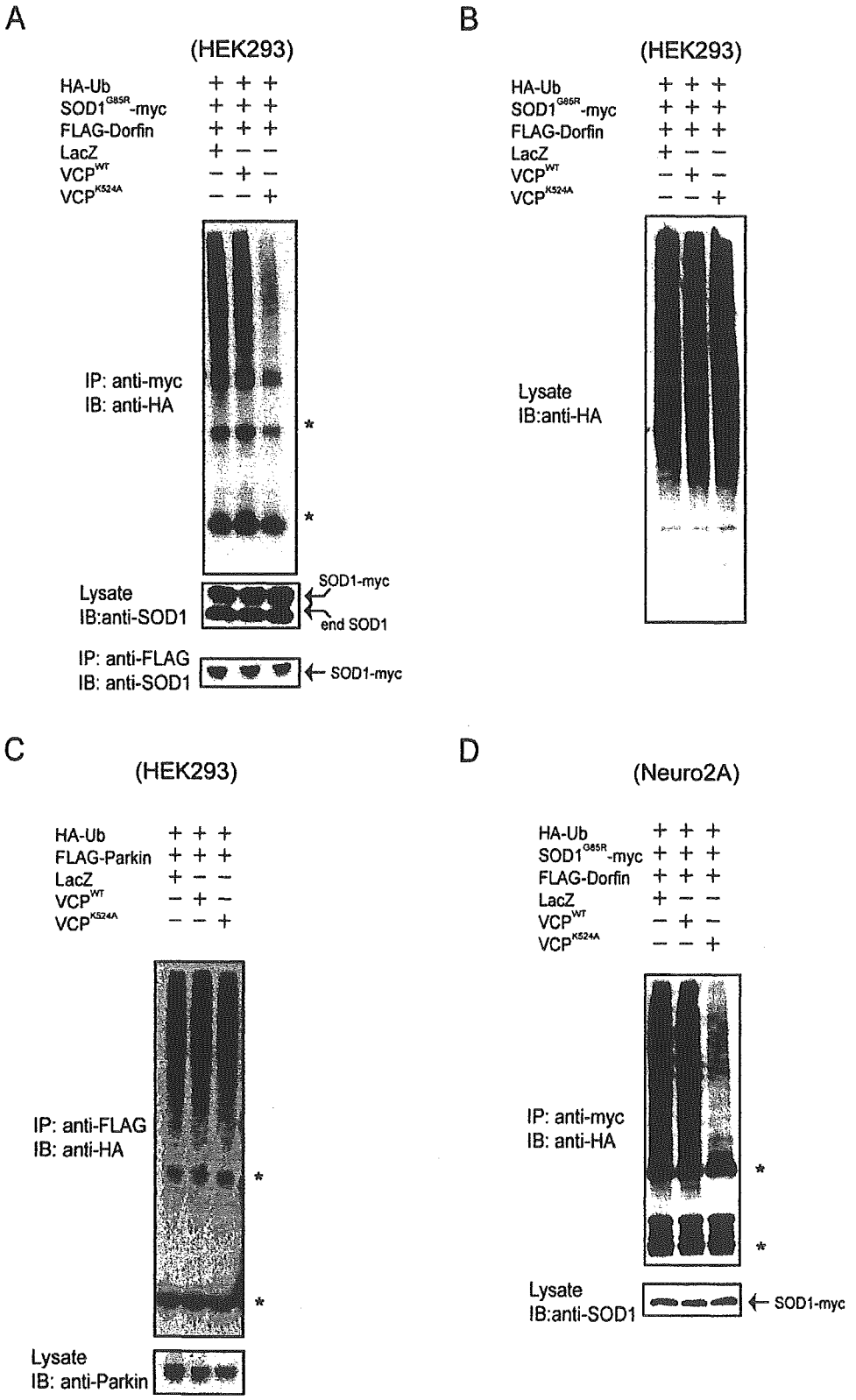

FIG. 7. **A dominant negative mutant of VCP, VCP^{K524A} inhibits the E3 ubiquitin ligase activity of Dorfin.** *A*, inhibition of dominant negative form mutant VCP^{K524A} on the E3 ubiquitin ligase activity of Dorfin. HEK293 cells were co-transfected with SOD1^{G85R}-Myc, HA-Ub, FLAG-Dorfin, and VCP^{WT}, VCP^{K524A}, or LacZ. Immunoprecipitation (*IP*) was performed with Myc antibody (9E10) and FLAG antibody (M2). *IB*, immunoblotting. *B*, neither VCP^{WT} nor VCP^{K524A} changed the level of total polyubiquitylated protein in the cell lysate. Ten percent of the volume of HEK293 cells used in *A* was subjected to immunoblotting using anti-HA (12CA5) antibody. *C*, autoubiquitylation of FLAG-Parkin was not influenced by the dominant negative form VCP^{K524A}. HEK293 cells were co-transfected with FLAG-Parkin, HA-Ub, and VCP^{WT}, VCP^{K524A}, or LacZ. Immunoprecipitation with FLAG antibody (M2) was performed. *D*, inhibition of VCP^{K524A} on E3 ubiquitin ligase activity of Dorfin in Neuro2a cells. Neuro2a cells were co-transfected with SOD1^{G85R}-Myc, HA-Ub, FLAG-Dorfin, and VCP^{WT}, VCP^{K524A}, or LacZ. Immunoprecipitation was performed using Myc antibody (9E10) and FLAG antibody (M2). The *asterisks* indicate IgG light and heavy chains.

The amount of Dorfin bound with VCP was saturated at even molar ratio *in vitro* (Fig. 3, *B* and *C*). Since VCP exists as a homohexamer (Fig. 3*D*), the *in vivo* observed size of ~600 kDa appears to be too small for the Dorfin-VCP complex if one VCP molecule binds to more than one Dorfin as shown in *in vitro* experiments. However, it is noteworthy that the size of molecules estimated by glycerol density gradient centrifugation analysis used in this study is not accurate and sufficient to discuss the molecular interaction of Dorfin and VCP in the cells. To date, various adaptor proteins, with which VCP forms multiprotein complexes, have been identified, such as Npl4, Ufd1 (18, 20), Ufd2 (34), Ufd3 (35), p47 (36), or SVIP (37). Although our *in vitro* study showed direct physical interaction between Dorfin and VCP, the environment with those adaptor proteins might reflect *in vivo* conditions. This also may explain the apparent discrepancy of the Dorfin-VCP binding fashions between *in vivo* and *in vitro* analyses.

Treatment with a proteasomal inhibitor causes the translocation of endogenous VCP and Dorfin to the aggresome in cultured cells (4, 15). Our results showed that these two proteins indeed colocalized perinuclearly in the aggresome following treatment with a proteasomal inhibitor (Fig. 4). Furthermore, we were able to demonstrate both Dorfin and VCP immunoreactivities in LB-like inclusions in ALS and LBs in PD (Fig. 5). In the majority of LBs, indistinguishable peripheral staining patterns were observed with both anti-Dorfin and anti-VCP antibodies. These results confirmed that both Dorfin and VCP are associated with the formation processes of aggresomes and inclusion bodies through physical interaction.

We showed here that co-expression of VCP^{K524A} resulted in a marked decrease of ubiquitylation activity of Dorfin compared with co-expression of VCP^{WT} or control. On the other hand, VCP^{K524A} failed to decrease autoubiquitylation activity of Parkin. VCP^{K524A} did not change the level of polyubiquitylated protein accumulation in the cell lysate in this study (Fig. 7). Knockdown experiments using the RNA interference technique showed accumulation of polyubiquitylated proteins (38). Combined with the observation that inhibition of VCP did not decrease the general accumulation of polyubiquitylated proteins, our results indicated that the E3 regulation function of VCP may be specific to certain E3 ubiquitin ligases such as Dorfin. VCP is an abundant protein that accounts for more than 1% of protein in the cell cytosol and is known to have various chaperone-like activities (39); therefore, it may function as a scaffold protein on the E3 activity of Dorfin. The localization of Dorfin and VCP in UBIs in various neurodegenerative disorders indicates the involvement of these proteins in the quality control system for abnormal proteins accumulated in the affected neurons in neurodegenerative disorders.

Since the unfolded protein response and ERAD are dynamic responses required for the coordinated disposal of misfolded proteins (40), the ERAD pathway can be critical for the etiology of neuronal cell death caused by various unfolded proteins. VCP is required for multiple aspects of the ERAD system by recognition of polyubiquitylated proteins and translocations to the 26 S proteasome for processive degradation through the VCP-Npl4-Ufd1 complex (18, 41). Our results suggest the involvement of Dorfin in the ERAD system, which is related to the pathogenesis of neurodegenerative disorders, such as PD or Alzheimer's disease. Further study including Dorfin knockout and/or knockdown models should examine the pathophysiology of Dorfin in association with the ERAD pathway or other cellular functions. Such studies should enhance our understanding of the pathogenetic role of Dorfin in neurodegenerative disorders.

REFERENCES

1. Julien, J. P. (2001) *Cell* **104,** 581–591
2. Rowland, L. P., and Shneider, N. A. (2001) *N. Engl. J. Med.* **344,** 1688–1700
3. Ishigaki, S., Niwa, J., Ando, Y., Yoshihara, T., Sawada, K., Doyu, M., Yamamoto, M., Kato, K., Yotsumoto, Y., and Sobue, G. (2002) *FEBS Lett.* **531,** 354–358
4. Niwa, J., Ishigaki, S., Doyu, M., Suzuki, T., Tanaka, K., and Sobue, G. (2001) *Biochem. Biophys. Res. Commun.* **281,** 706–713
5. Niwa, J., Ishigaki, S., Hishikawa, N., Yamamoto, M., Doyu, M., Murata, S., Tanaka, K., Taniguchi, N., and Sobue, G. (2002) *J. Biol. Chem.* **277,** 36793–36798
6. Ciechanover, A., and Brundin, P. (2003) *Neuron* **40,** 427–446
7. Hishikawa, N., Niwa, J., Doyu, M., Ito, T., Ishigaki, S., Hashizume, Y., and Sobue, G. (2003) *Am. J. Pathol.* **163,** 609–619
8. Mayer, R. J., Lowe, J., Lennox, G., Doherty, F., and Landon, M. (1989) *Prog. Clin. Biol. Res.* **317,** 809–818
9. Johnston, J. A., Ward, C. L., and Kopito, R. R. (1998) *J. Cell Biol.* **143,** 1883–1898
10. Kopito, R. R. (2000) *Trends Cell Biol.* **10,** 524–530
11. Kobayashi, T., Tanaka, K., Inoue, K., and Kakizuka, A. (2002) *J. Biol. Chem.* **277,** 47358–47365
12. Shimura, H., Hattori, N., Kubo, S., Mizuno, Y., Asakawa, S., Minoshima, S., Shimizu, N., Iwai, K., Chiba, T., Tanaka, K., and Suzuki, T. (2000) *Nat. Genet.* **25,** 302–305
13. Fukuchi, M., Imamura, T., Chiba, T., Ebisawa, T., Kawabata, M., Tanaka, K., and Miyazono, K. (2001) *Mol. Biol. Cell* **12,** 1431–1443
14. Ishigaki, S., Liang, Y., Yamamoto, M., Niwa, J., Ando, Y., Yoshihara, T., Takeuchi, H., Doyu, M., and Sobue, G. (2002) *J. Neurochem.* **82,** 576–584
15. Hirabayashi, M., Inoue, K., Tanaka, K., Nakadate, K., Ohsawa, Y., Kamei, Y., Popiel, A. H., Sinohara, A., Iwamatsu, A., Kimura, Y., Uchiyama, Y., Hori, S., and Kakizuka, A. (2001) *Cell Death Differ.* **8,** 977–984
16. Natsume, T., Yamauchi, Y., Nakayama, H., Shinkawa, T., Yanagida, M., Takahashi, N., and Isobe, T. (2002) *Anal. Chem.* **74,** 4725–4733
17. Matsuda, N., Suzuki, T., Tanaka, K., and Nakano, A. (2001) *J. Cell Sci.* **114,** 1949–1957
18. Bays, N. W., and Hampton, R. Y. (2002) *Curr. Biol.* **12,** R366–R371
19. Ye, Y., Meyer, H. H., and Rapoport, T. A. (2001) *Nature* **414,** 652–656
20. Braun, S., Matuschewski, K., Rape, M., Thoms, S., and Jentsch, S. (2002) *EMBO J.* **21,** 615–621
21. Jarosch, E., Taxis, C., Volkwein, C., Bordallo, J., Finley, D., Wolf, D. H., and Sommer, T. (2002) *Nat. Cell Biol.* **4,** 134–139
22. Rabinovich, E., Kerem, A., Frohlich, K. U., Diamant, N., and Bar-Nun, S. (2002) *Mol. Cell. Biol.* **22,** 626–634
23. Mizuno, Y., Hori, S., Kakizuka, A., and Okamoto, K. (2003) *Neurosci. Lett.* **343,** 77–80
24. Ito, T., Niwa, J., Hishikawa, N., Ishigaki, S., Doyu, M., and Sobue, G. (2003) *J. Biol. Chem.* **278,** 29106–29114
25. Meyer, H. H., Kondo, H., and Warren, G. (1998) *FEBS Lett.* **437,** 255–257
26. Kondo, H., Rabouille, C., Newman, R., Levine, T. P., Pappin, D., Freemont, P., and Warren, G. (1997) *Nature* **388,** 75–78
27. Rabouille, C., Kondo, H., Newman, R., Hui, N., Freemont, P., and Warren, G. (1998) *Cell* **92,** 603–610
28. Hetzer, M., Meyer, H. H., Walther, T. C., Bilbao-Cortes, D., Warren, G., and Mattaj, I. W. (2001) *Nat. Cell Biol.* **3,** 1086–1091
29. Frohlich, K. U., Fries, H. W., Rudiger, M., Erdmann, R., Botstein, D., and Mecke, D. (1991) *J. Cell Biol.* **114,** 443–453
30. Asai, T., Tomita, Y., Nakatsuka, S., Hoshida, Y., Myoui, A., Yoshikawa, H., and Aozasa, K. (2002) *Jpn. J. Cancer Res.* **93,** 296–304
31. Kawaguchi, Y., Okamoto, T., Taniwaki, M., Aizawa, M., Inoue, M., Katayama, S., Kawakami, H., Nakamura, S., Nishimura, M., Akiguchi, I., Kimura, J., Narumiya, S., and Kakizuka, A. (1994) *Nat. Genet.* **8,** 221–228
32. Matsumoto, M., Yada, M., Hatakeyama, S., Ishimoto, H., Tanimura, T., Tsuji, S., Kakizuka, A., Kitagawa, M., and Nakayama, K. I. (2004) *EMBO J.* **23,** 659–669
33. Watts, G. D., Wymer, J., Kovach, M. J., Mehta, S. G., Mumm, S., Darvish, D., Pestronk, A., Whyte, M. P., and Kimonis, V. E. (2004) *Nat. Genet.* **36,** 377–381
34. Koegl, M., Hoppe, T., Schlenker, S., Ulrich, H. D., Mayer, T. U., and Jentsch, S. (1999) *Cell* **96,** 635–644
35. Ghislain, M., Dohmen, R. J., Levy, F., and Varshavsky, A. (1996) *EMBO J.* **15,** 4884–4899
36. Meyer, H. H., Wang, Y., and Warren, G. (2002) *EMBO J.* **21,** 5645–5652
37. Nagahama, M., Suzuki, M., Hamada, Y., Hatsuzawa, K., Tani, K., Yamamoto, A., and Tagaya, M. (2003) *Mol. Biol. Cell* **14,** 262–273
38. Wojcik, C., Yano, M., and DeMartino, G. N. (2004) *J. Cell Sci.* **117,** 281–292
39. Dalal, S., and Hanson, P. I. (2001) *Cell* **104,** 5–8
40. Travers, K. J., Patil, C. K., Wodicka, L., Lockhart, D. J., Weissman, J. S., and Walter, P. (2000) *Cell* **101,** 249–258
41. Dai, R. M., and Li, C. C. (2001) *Nat. Cell Biol.* **3,** 740–744

EMBO reports

scientific report

Parkin binds the Rpn10 subunit of 26S proteasomes through its ubiquitin-like domain

Eri Sakata[1], Yoshiki Yamaguchi[1], Eiji Kurimoto[1], Jun Kikuchi[2], Shigeyuki Yokoyama[2,3], Shingo Yamada[4], Hiroyuki Kawahara[4], Hideyoshi Yokosawa[4], Nobutaka Hattori[5], Yoshikuni Mizuno[5], Keiji Tanaka[6] & Koichi Kato[1,2+]

[1]Department of Structural Biology and Biomolecular Engineering, Graduate School of Pharmaceutical Sciences, Nagoya City University, Nagoya, Japan; [2]Genomic Sciences Centre, RIKEN Yokohama Institute, Yokohama, Japan; [3]Department of Biophysics and Biochemistry, Graduate School of Science, University of Tokyo, Tokyo, Japan; [4]Department of Biochemistry, Graduate School of Pharmaceutical Sciences, Hokkaido University, Sapporo, Japan; [5]Department of Neurology, School of Medicine, Juntendo University, Tokyo, Japan & [6]Department of Molecular Oncology, Tokyo Metropolitan Institute of Medical Science, Tokyo, Japan

Parkin, a product of the causative gene of autosomal-recessive juvenile parkinsonism (AR-JP), is a RING-type E3 ubiquitin ligase and has an amino-terminal ubiquitin-like (Ubl) domain. Although a single mutation that causes an Arg to Pro substitution at position 42 of the Ubl domain (the Arg 42 mutation) has been identified in AR-JP patients, the function of this domain is not clear. In this study, we determined the three-dimensional structure of the Ubl domain of parkin by NMR, in particular by extensive use of backbone ^{15}N-^{1}H residual dipolar-coupling data. Inspection of chemical-shift-perturbation data showed that the parkin Ubl domain binds the Rpn10 subunit of 26S proteasomes via the region of parkin that includes position 42. Our findings suggest that the Arg 42 mutation induces a conformational change in the Rpn10-binding site of Ubl, resulting in impaired proteasomal binding of parkin, which could be the cause of AR-JP.

EMBO reports 4, 301–306 (2003)
doi:10.1038/sj.embor.embor764

INTRODUCTION

Autosomal-recessive juvenile parkinsonism (AR-JP), one of the most common forms of familial Parkinson's disease, is characterized by selective and massive loss of dopaminergic neurons in the substantia nigra of the midbrain and by the absence of Lewy bodies (cytoplasmic inclusion bodies), which consist of aggregates of abnormally accumulated proteins (Yamamura *et al.*, 1973). The causative gene of AR-JP, *parkin*, encodes a 52-kDa protein composed of three parts: the amino-terminal ubiquitin (Ub)-like domain (Ubl), the carboxy-terminal RING-finger box and the linker region, which connects the two domains (Kitada *et al.*, 1998). Recently, parkin was shown to be a RING-type ubiquitin ligase (or E3 protein) that catalyses protein ubiquitylation, leading to proteasome-mediated protein degradation (Imai *et al.*, 2000; Shimura *et al.*, 2000; Zhang *et al.*, 2000). Analysis of *parkin* mutations in AR-JP patients has revealed that the molecular basis of this disease is the loss of parkin E3-enzyme function in the ubiquitin–proteasome pathway, which may result in the accumulation of parkin substrates in neurons (Chung *et al.*, 2001; Imai *et al.*, 2001; Shimura *et al.*, 2001).

The C-terminal RING box serves as a recruiting motif for ubiquitin-conjugating enzymes (E2 enzymes), such as Ubc4, Ubc7, UbcH7 and UbcH8, whereas the functional role of the N-terminal Ubl domain is poorly characterized. The number of identified mutations in the *parkin* gene in patients with early-onset parkinsonism has recently increased (Lücking *et al.*, 2000), and a single mutation that causes an Arg to Pro substitution at amino-acid position 42 of the Ubl domain has been identified in one family of AR-JP patients (Terreni *et al.*, 2001). This mutated parkin protein retains the ability to bind UbcH7, but fails to co-immunoprecipitate ubiquitylated proteins such as *O*-glycosylated α-synuclein (Shimura *et al.*, 2001). These data suggest that the Ubl domain contributes to the recognition of target proteins.

However, accumulating evidence indicates that various proteins with Ubl domains, such as Rad23, Dsk2 and their human homologues (HR23a/b and PLIC1/2, respectively), provide links between 26S proteasomes and the ubiquitylation machinery (Hiyama *et al.*, 1999; Kleijnen *et al.*, 2000; Wilkinson *et al.*, 2001). All of these proteins have Ubl domains at their N termini, and ubiquitin-associated (UBA) domains at their C termini; the Ubl domains are able to interact

[1]Department of Structural Biology and Biomolecular Engineering, Graduate School of Pharmaceutical Sciences, Nagoya City University, 3-1 Tanabe-dori, Mizuho-ku, Nagoya 467-8603, Japan; [2]Genomic Sciences Center, RIKEN Yokohama Institute, 1-7-29 Suehiro-cho, Tsurumi-ku, Yokohama 230-0045, Japan; [3]Department of Biophysics and Biochemistry, Graduate School of Science, University of Tokyo, 7-3-1 Hongo, Bunkyo-ku, Tokyo 113-0033, Japan; [4]Department of Biochemistry, Graduate School of Pharmaceutical Sciences, Hokkaido University, Sapporo 060-0812, Japan; [5]Department of Neurology, School of Medicine, Juntendo University, 2-1-1 Hongo, Bunkyo-ku, Tokyo 113-0033, Japan & [6]Department of Molecular Oncology, Tokyo Metropolitan Institute of Medical Science, 3-18-22 Honkomagome, Bunkyo-ku, Tokyo 113-8613, Japan
+Corresponding author. Tel/Fax: +81 52 836 3447;
E-mail: kkato@phar.nagoya-cu.ac.jp

Received 29 August 2002; revised 5 December 2002; accepted 17 December 2002
Published online 21 February 2003

with 26S proteasomes, whereas the UBA domains can bind to polyubiquitin chains (Buchberger, 2002). However, it has been reported that a 50-kDa subunit of human 26S proteasomes, originally called S5a, can bind to polyubiquitin conjugates *in vitro*, and could therefore possibly function as a polyubiquitin-binding subunit (Deveraux *et al.*, 1994). Several S5a homologues (such as Mbp1, Mcb1, Sun1, Pus1, μ-54 and Rpn1) have been identified in various eukaryotes (Kawahara *et al.*, 2000). Here, we call S5a and its homologues 'Rpn10' on the basis of a recent proposal (Finley *et al.*, 1998). Intriguingly, Rpn10 also binds the Ubl domains of HR23a/b and PLIC2 (Hiyama *et al.*, 1999; Walters *et al.*, 2002). Mutagenesis studies have shown that Rpn10 has two highly conserved polyubiquitin-binding sites, PUbS1 and PUbS2, each of which contains five hydrophobic residues forming an alternating pattern of large and small side-chains (Young *et al.*, 1998). In addition, a homologous motif with a similar structure, known as a ubiquitin-interacting motif (UIM), which physically interacts with ubiquitin and/or polyubiquitylated chains, was recently identified in various proteins (Hofmann & Falquet, 2001). NMR studies have shown that the Ubl domains of HR23a and PLIC2 share a highly conserved hydrophobic surface for binding Rpn10 (Walters *et al.*, 2002). In the Ubl domain of parkin, some of the residues corresponding to those in the hydrophobic Rpn10-binding surface are substituted with polar residues. Therefore, one cannot predict whether parkin can bind 26S proteasomes through interaction with the Rpn10 subunit.

In this study, we have determined the three-dimensional (3D) structure of the Ubl domain of parkin by NMR spectroscopy. Based on chemical-shift-perturbation data, we provide evidence that Ubl interacts with Rpn10 using a surface almost identical to the Rpn10-binding surfaces of the Ubl domains of HR23a and PLIC2. The Rpn10-binding site determined in this study includes position 42 of the parkin Ubl domain. We also discuss how these results relate to the molecular cause of AR-JP.

Table 1 | Statistics for NMR structure calculations

Overhauser-effect distance restraints	
Total number	489
Inter-residue	159
Medium range	71
Long range	66
Intra-residue	193
Number of hydrogen bonds	20
Number of residual dipolar-coupling restraints	129
Dihedral-angle restraints	
ϕ	41
ψ	41
Mean r.m.s. deviation of backbone atoms from the average structure (Å)	0.371 ± 0.117
Mean r.m.s. deviation of all heavy atoms from the average structure (Å)	1.025 ± 0.086
Deviation from idealized covalent geometry	
Bonds (Å)	0.005 ± 0.000
Angles (°)	0.684 ± 0.012
Impropers (°)	0.697 ± 0.012
Ramachandran plot (%)	
Residues in most favourable region	69.1
Residues in additionally allowed region	26.5
Residues in generously allowed region	4.4
Residues in disallowed region	0

RESULTS AND DISCUSSION

The solution structure of the parkin Ubl domain

The Ubl domain of parkin, comprising residues 1–76 of the full-length protein, was produced as a recombinant protein in *Escherichia coli*. Preliminary NMR studies revealed that the Ubl domain forms a disulphide-linked dimer, causing a large amount of aggregation during spectral measurement. Therefore, the solution conditions were optimized by adding 10 mM [$^2H_{10}$] dithiothreitol (DTT). However, the concentration of Ubl never exceeded 0.1 mM, even under these reducing conditions. Therefore, we carried out all spectral measurements using the parkin Ubl domain at a concentration of 0.1 mM. Gel-filtration analysis showed that the Ubl domain was monomeric in the solution conditions used (data not shown). Because extensive collection of the inter-proton restraints based on the nuclear Overhauser enhancement spectroscopy (NOESY) spectra was difficult to carry out, due to dilution of the sample solution (approximately 5–10% of the concentration typically used), the structure determination relied heavily on orientational restraints with respect to the NMR magnetic field. We chose two orientational media: bicelle and cetyltriammonium bromide (CTAB)-doped bicelle (see Methods) for measuring the backbone ^{15}N-^1H residual dipolar couplings (RDCs). The NMR data used for structure calculations are summarized in Table 1. A final set of ten structures was selected for 50 restrained molecular dynamics calculations for the Ubl domain, based on agreement with the experimental data and overall structural quality according to the following prerequisites: no nuclear Overhauser effect (NOE) violations >0.5 Å, no torsion angle violation >5° and no RDC violations >2 Hz (over a 0.6 Hz range) (Fig. 1A). The secondary structure of the parkin Ubl domain consists of two α-helices (α1: residues Ile 23–Arg 33; α2: Gln 57–Asp 60) and five β-sheets (β1: Ile 2–Phe 7; β2: His 11–Val 15; β3: Arg 42–Phe 45; β4: Lys 48–Glu 49; β5: Gln 64–Val 70). These are arranged in a typical ubiquitin fold (Fig. 1B and C). The average r.m.s. deviations from the average structure within the secondary structural elements for backbone atoms and for all heavy atoms are 0.371 Å and 1.025 Å, respectively.

Interaction of the parkin Ubl domain with Rpn10

To analyse the interaction of Rpn10 with the Ubl domain of parkin, we used the Rpn10 fragment comprising residues 196–306 ($Rpn10_{196-306}$), which retains both PUbS1 and PUbS2. Figure 2A shows a comparison of the ^1H-^{15}N heteronuclear single-quantum coherence (HSQC) spectra of the uniformly-[^{15}N]-labelled Ubl domain in the presence and absence of $Rpn10_{196-306}$. Twenty-one significantly perturbed amide resonances were observed, whereas the rest of the spectrum remained unchanged, indicating the formation of a specific complex between Ubl and $Rpn10_{196-306}$ (Fig. 2B). The perturbed residues were mapped onto the Ubl domain structure (Fig. 2C). The identified contact-surface comprised the β3 and β4 strands of the parkin Ubl domain and the residues in their spatial proximity, which corresponds with the Rpn10-binding surfaces of the Ubl domains of PLIC2 and HR23a (Walters *et al.*, 2002).

The Rpn10-binding sites of PLIC2 and HR23a have been characterized by the surface clusters of the hydrophobic residues that are bound by basic residues on the molecular surface, whereas the ubiquitin-binding site of Rpn10 seems to be a hydrophobic area bound by acidic residues (Walters *et al.*, 2002). In PLIC2, the hydrophobic cluster comprises residues Ile 75, Ala 77, Ile 80, Val 101 and Ile 102, which correspond to Ile 44, Ala 46, Glu 49, Val 70 and Gln 71, respectively, in parkin. Mutagenesis studies have shown that hydrophobicity at

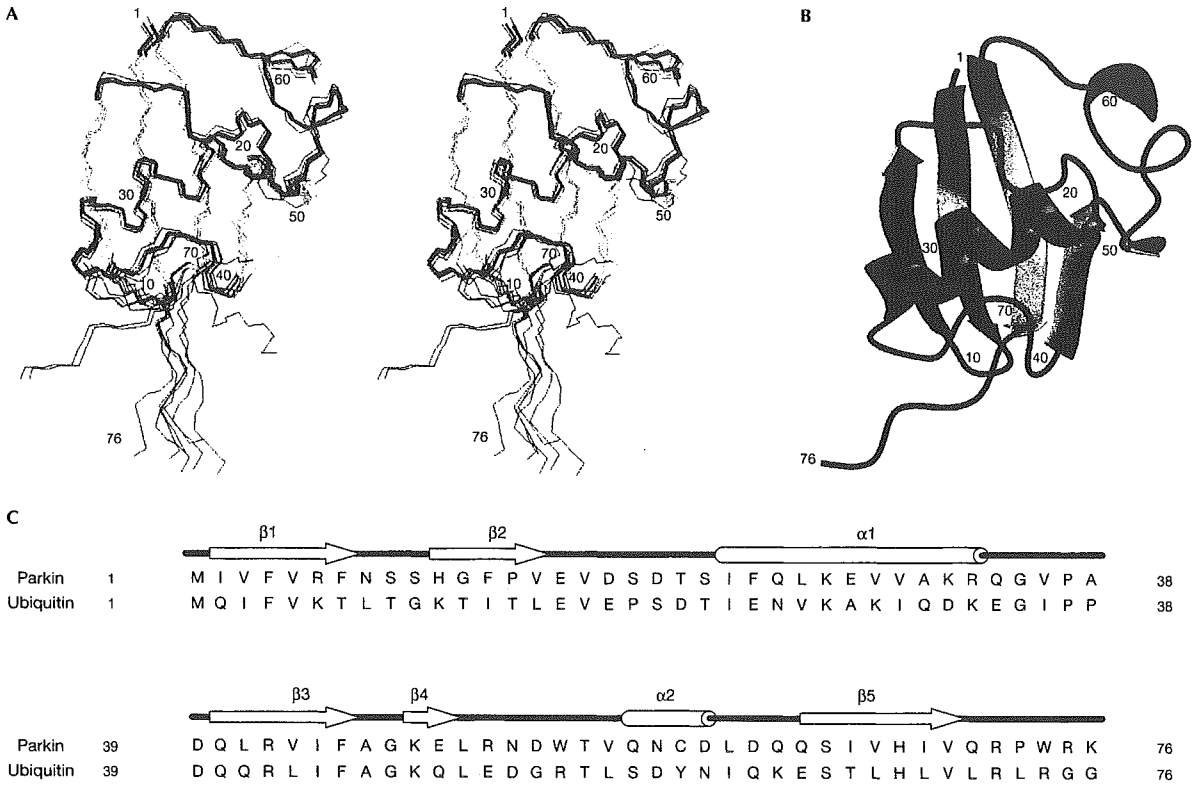

Fig. 1 | The solution structure of the ubiquitin-like (Ubl) domain of parkin. (A) Stereo view of ten converged structures of the parkin Ubl domain. **(B)** Ribbon representation of the average structure. β-strands and α-helices are coloured yellow and pink, respectively, in **(A)** and **(B)**. Numbers in **(A)** and **(B)** indicate amino-acid positions in the Ubl domain sequence. **(C)** Sequence alignment and secondary-structure elements of the parkin Ubl domain and ubiquitin.

amino-acid position 8 in tetraubiquitin is required for its binding to Rpn10 (Beal *et al.*, 1998). Position 8 is occupied by Leu, Pro and Asn in ubiquitin, PLIC2 and parkin, respectively. It should be noted that parkin also has the ability to bind Rpn10, using the surface area corresponding to the hydrophobic cluster of PLIC2 and HR23a, notwithstanding the fact that half of the positions in this cluster are occupied by polar residues in parkin. On the basis of the NMR data from this study, we suggest that interactions between the Rpn10 and Ubl domains are not soley due to the hydrophobic properties of the Ubl domains. It is possible that the relative contributions of the two ubiquitin-binding sites, PUbS1 and PUbS2, are different when binding to different Ubl domains. Indeed, little or no chemical-shift-perturbation was observed for the Ubl domain of parkin after addition of PUbS1 or PUbS2 alone (data not shown). This is in contrast with the finding that the PUbS2 region can interact with the Ubl domain of PLIC2 and HR23a (Walters *et al.*, 2002), suggesting that the modes of the interactions between the Rpn10 and Ubl domains are different, depending on the particular Ubl-domain-containing protein.

Several lines of evidence suggest that E3 proteins associate with 26S proteasomes, thereby recruiting the ubiquitylation machinery (Xie & Varshavsky, 2000; Jäger *et al.*, 2001). The NMR data presented here show the structural basis for the proteasomal binding of E3. Recent studies suggest that the ATPase subunit of 26S proteasomes, not the Rpn10 subunit, is responsible for binding to the polyubiquitin chain (Lam *et al.*, 2002). Taking the data in the present study into consideration, we suggest that parkin and a polyubiquitin-tagged substrate come together on 26S proteasomes to form an efficient assembly line for protein degradation.

Our preliminary experiments revealed that a region of endogenous parkin was co-immunoprecipitated with 26S proteasomes in extracts from Nero2a cells and from mouse brain extracts (data not shown), suggesting that parkin interacts with 26S proteasomes, presumably through the Rpn10 subunit. However, detection of a physical interaction between a glutathione-*S*-transferease (GST)-fused Ubl domain of parkin and FLAG-tagged Rpn10 by co-immunoprecipitation/western blot analysis was unsuccessful, although a clear interaction between HR23a and Rpn10 was seen under the same conditions (see supplementary information online), indicating that the parkin–Rpn10 interaction is weak. Alternatively, it is possible that tagging of parkin and Rpn10 may prevent any interaction between them under *in vitro* conditions. However, in yeast, other proteasome subunits—Rpn1 and/or Rpn2—also bind the ubiquitin-like domain of Rad23 (the yeast

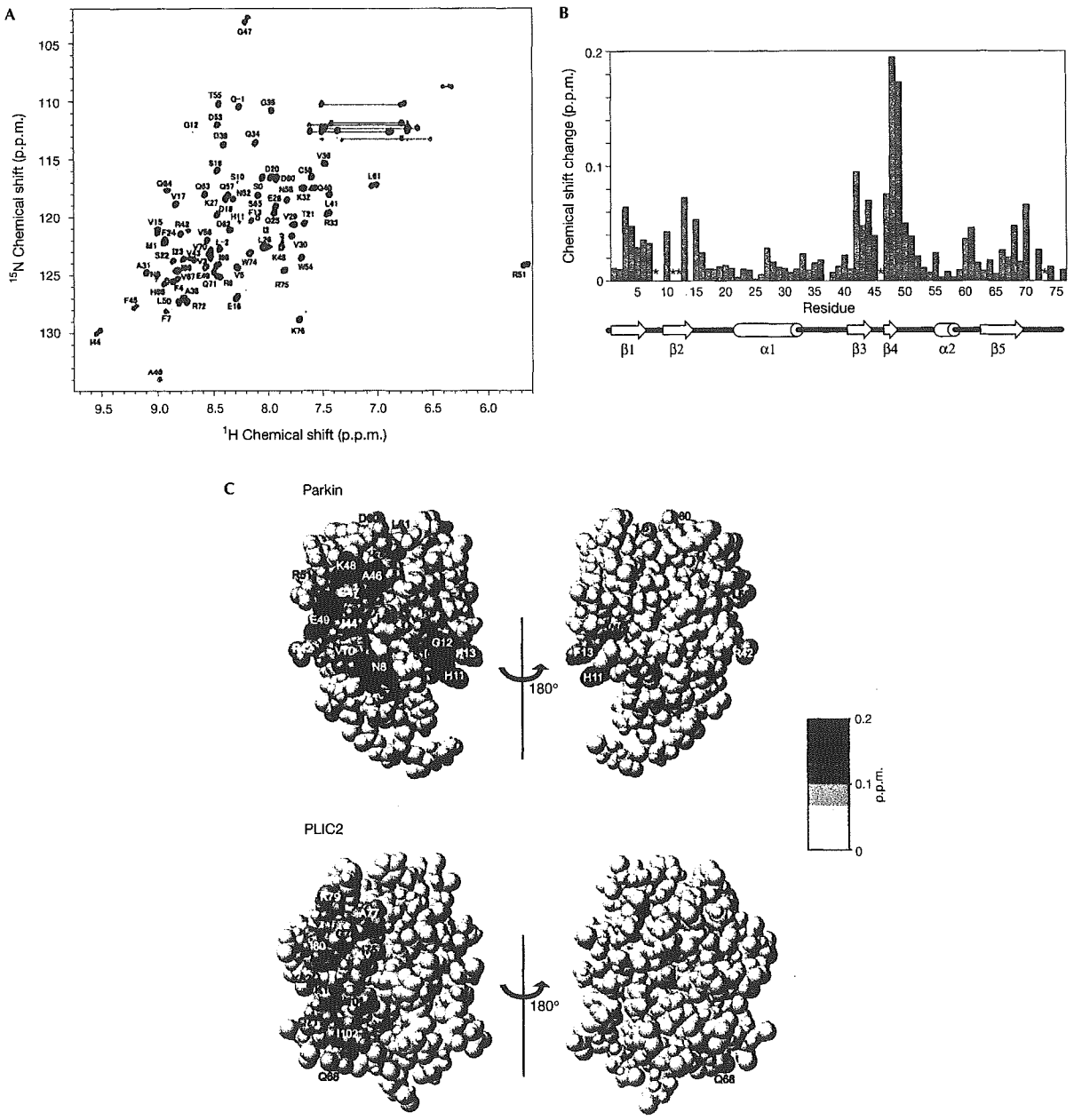

Fig. 2 | Identification of the binding site for $Rpn10_{196-306}$ in the parkin ubiquitin-like (Ubl) domain. (A) ^{1}H-^{15}N heteronuclear single-quantum coherence (HSQC) spectrum of the parkin Ubl domain in the presence (red) and absence (black) of equimolar quantities of $Rpn10_{196-306}$. The peaks labelled with L-2, G-1 and S0 originate from the amino-terminal tag. (B) NMR chemical-shift-perturbation data for the parkin Ubl domain. The data are displayed for each residue according to the equation $(0.2\,\delta_N^2 + \delta_H^2)^{1/2}$, where δ_N and δ_H represent the change in nitrogen and proton chemical shifts on addition of $Rpn10_{196-306}$. Asterisks indicate residues the peaks of which became undetectable due to broadening. Secondary structure elements for the parkin Ubl are shown below the graph. (C) Mapping of the perturbed residues of the Ubl domains of parkin and PLIC2 (Walters *et al.*, 2002) on binding to Rpn10. Residues showing a chemical-shift-perturbation are coloured in red, with the colour gradient indicating the strength of the perturbation. Residues the peaks of which became undetectable on binding to Rpn10 are shown in purple.

homologue of HR23a), when only Rpn1 and/or Rpn2 are assembled into the 26S proteasome complex (Elsasser *et al.*, 2002; Saeki *et al.*, 2002). Therefore, the possibility of an interaction of parkin with Rpn1 and/or Rpn2, as well as with Rpn10, cannot be excluded. It is of note that yeast Rpn10 lacks the PUbS2 sequence (Kawahara *et al.*, 2000) and that the human PUbS2 region, but not the PUbS1 region, can only interact with HR23a (Hiyama *et al.*, 1999). However, it is unclear whether the 26S proteasome subunit(s) that functions as a Ubl-domain acceptor has changed during evolution. The determination of whether both Rpn1/Rpn2 and Rpn10 function redundantly as Ubl-domain acceptors, or whether they have distinct functions, awaits further studies.

SPECULATION

The NMR data presented here indicate that the Arg 42 residue of parkin is located in the Rpn10-binding site. One family of AR-JP patients have a point mutation at position 42 (Terreni *et al.*, 2001), in which Arg is substituted with Pro. It is possible that this mutation induces a significant conformational change in the Rpn10-binding site of the parkin Ubl domain, resulting in impaired proteasomal binding by parkin. Indeed, mutant parkin carrying the Arg-42-Pro mutation was extremely difficult to dissolve at a submillimolar concentration for NMR analysis (data not shown); this insolubility might be associated with loss of the correct functional conformation in the mutant form of parkin. We suggest that this defect hampers the formation of an efficient assembly line for protein degradation, and thereby causes the accumulation of parkin substrates in neurons, leading to Parkinson's disease.

METHODS

Protein expression. The DNA fragment encoding the Ubl domain (amino acids 1–76) of human parkin was cloned into the pGEX-6P-3 vector (Amersham Biosciences) with an N-terminal GST moiety. For expression, the plasmid was cotransformed with the pLysS plasmid (Novagen) into the BL21(DE3)CodonPlus *E. coli* strain (Stratagene). For the production of isotopically labelled protein, cells were grown in M9 minimal media containing [^{15}N]NH_4Cl (1 g l^{-1}) and [u-^{13}C]glucose (2 g l^{-1}). The GST-fusion protein was purified from cell lysates using a glutathione-sepharose column. The fusion protein was cleaved by incubation with 3 units of PreScission protease (Amersham Biosciences) for each milligram of GST-fusion protein for 16 h at 4 °C. GST was removed by the application of the digested products onto a second glutathione-sepharose column. Further purification of the protein was carried out using a Superose12 gel-filtration column (Amersham Biosciences). DNA encoding mouse $Rpn10_{196-306}$ was cloned into the pGEX-6P-1 vector. For expression of $Rpn10_{196-306}$, the plasmid was transformed into the *E. coli* BL21(DE3)CodonPlus strain, and cells were grown in Luria–Bertani media. The expression and purification protocols for $Rpn10_{196-306}$ were generally the same as those used for the parkin Ubl domain.

NMR spectroscopy. NMR samples were prepared at a concentration of 0.1 mM in 90% H_2O/10% ^2H_2O (v/v), 50 mM potassium phosphate buffer, 10 mM [$^2H_{10}$]DTT, pH 6.0. All NMR spectra were recorded at 303 K using Bruker DRX800 or DMX500 spectrometers equipped with 5-mm inverse triple-resonance probes with three-axis gradient coils. Backbone and Cβ resonances were assigned sequentially using the following techniques: two-dimensional (2D) ^{1}H-^{15}N HSQC, constant-time-^{1}H-^{13}C HSQC, and 3D HNCA, HN(CO)CA, HNCO, CBCA(CO)NH and CBCANH spectra. Side-chain and Hα assignments were obtained from HBHA(CO)NH, HBHANH, ^{15}N-edited total-correlation spectroscopy (TOCSY), ^{15}N-edited NOESY, ^{13}C-edited NOESY, HCACO, HCCH-COSY and HCCH-TOCSY spectra. Distance restraints for the parkin Ubl domain were obtained by using ^{15}N-edited NOESY and ^{13}C-edited NOESY spectra. For measurements of residual dipolar couplings, the anisotropic medium used was a nematic-phase liquid-crystalline state, induced by bicelle and cetyltriammonium bromide (CTAB)-doped bicelle (Ottiger & Bax, 1998). The final optimized bicelle concentration for both media was 5% (w/w) for 0.1 mM of the parkin Ubl domain. The 2D ^{1}H-coupled ^{1}H-^{15}N HSQC experiments were used to measure the one-bond ^{15}N-^{1}H scalar coupling ($^1J_{NH}$) values in the isotropic state (in the absence of the liquid-crystalline media) and in the anisotropic media (in the presence of the bicelle or CTAB-doped bicelle). Initial estimates for the axial component of the molecular alignment tensor (*Da*) and the rhombicity (*R*) were obtained from the powder-pattern distribution of the overall ^{15}N-^{1}H RDC ($^1D_{NH}$) values (Clore *et al.*, 1998). These values were then optimized in a stepwise manner, using the calculated solution-structure of the parkin Ubl domain as described previously (Kikuchi *et al.*, 2002). The final values of *Da* and *R* for the parkin Ubl domain were 12 Hz and 0.21, respectively, for the bicelle media, and 18 Hz and 0.42, respectively, for the CTAB-doped bicelle media. Data processing and analysis was carried out using a Silicon Graphics O2 workstation with XWINNMR. The ^{1}H chemical shifts were referenced to external 4,4-dimethyl-4-silapentane-1-sulphonic acid.

Structural determination. Initial calculations were carried out with the NOE-derived inter-proton distance restraints, and with the backbone ϕ and ψ torsion angles restrained by the program TALOS (Cornilescu *et al.*, 1999), and hydrogen-bond restraints in the secondary-structure region. The inter-proton restraints were classified into three categories: 1.8–2.7 Å, 1.8–3.5 Å and 1.8–5.0 Å, corresponding to strong, medium and weak NOE intensities, respectively. The hydrogen-bond restraints (two per hydrogen bond) were set to rNH-O = 1.7–2.3 Å and rN-O = 2.7–3.3 Å, according to the ^{1}H-^{2}H exchange rate for the amide protons, TALOS-based secondary structure identification and the backbone NOE. The RDC-derived restraints were used in the SANI modules (Clore *et al.*, 1998) for performing a direct refinement against the measured dipolar-couplings with the program CNS version 1.1 (Brünger *et al.*, 1998). The calculations were started with extended structures (Nilges *et al.*, 1988), and consisted of a torsion angle space dynamics (TAD) measurement, followed by a Cartesian minimization (Stein *et al.*, 1997). The TAD consisted of 2,000 molecular dynamics steps of 15 picoseconds, carried out at 50,000 K, and a cooling phase (50,000 steps of 5 femtoseconds each) with annealing temperatures from 50,000 K to 0 K. A second TAD cooling-phase, consisting of 10,000 steps of 2 femtoseconds each, was applied, with annealing temperatures from 500 K to 0 K.

The final energy minimization was performed with the following force constants: 1,000 kcal mol^{-1} $Å^{-2}$ for bond lengths, 500 kcal mol^{-1} rad^{-2} for angles and improper torsions (which served to maintain planarity and chirality), 4 kcal mol^{-1} $Å^{-4}$ for the quartic van der Waals repulsion term, 10 kcal mol^{-1} $Å^{-2}$ for the experimental distance restraints, and 0.2 kcal mol^{-1} Hz^{-2} for the $^1D_{NH}$ RDC restraints. The stereochemical quality of the structures of the parkin Ubl domain were assessed using the program PROCHECK-NMR (Laskowski *et al.*, 1996). Graphic figures were generated by the program MOLMOL (Koradi *et al.*, 1996).

Supplementary information is available at *EMBO reports* online (http://www.emboreports.org)

ACKNOWLEDGEMENTS

This work was supported in part by the Yamanouchi Foundation for Research on Metabolic Disorders, by the Naito Foundation and by a Grant-in-Aid for Scientific Research on Priority Areas from the Ministry of Education, Science, Sports and Culture, Japan. The atomic coordinates have been deposited in the RCSB Protein Data Bank (accession code 1IYF).

REFERENCES

Beal, R.E., Toscano-Cantaffa, D., Young, P., Rechsteiner, M. & Pickart, C.M. (1998) The hydrophobic effect contributes to polyubiquitin chain recognition. *Biochemistry*, **37**, 2925–2934.

Brünger, A.T. *et al.* (1998) Crystallography & NMR system: A new software suite for macromolecular structure determination. *Acta Crystallogr. D Biol. Crystallogr.*, **54**, 905–921.

Buchberger, A. (2002) From UBA to UBX: new words in the ubiquitin vocabulary. *Trends Cell Biol.*, **12**, 216–221.

Chung, K.K. *et al.* (2001) Parkin ubiquitinates the alpha-synuclein-interacting protein, synphilin-1: implications for Lewy-body formation in Parkinson disease. *Nature Med.*, **7**, 1144–1150.

Clore, G.M., Gronenborn, A.M. & Bax, A. (1998) A robust method for determining the magnitude of the fully asymmetric alignment tensor of oriented macromolecules in the absence of structural information. *J. Magn. Reson.*, **133**, 216–221.

Cornilescu, G., Delaglio, F. & Bax, A. (1999) Protein backbone angle restraints from searching a database for chemical shift and sequence homology. *J. Biomol. NMR*, **13**, 333–347.

Deveraux, Q., Ustrell, V., Pickart, C. & Rechsteiner, M. (1994) A 26 S protease subunit that binds ubiquitin conjugates. *J. Biol. Chem.*, **269**, 7059–7061.

Elsasser, S. *et al.* (2002) Proteasome subunit Rpn1 binds ubiquitin-like protein domains. *Nature Cell Biol.*, **4**, 725–730.

Finley, D. *et al.* (1998) Unified nomenclature for subunits of the *Saccharomyces cerevisiae* proteasome regulatory particle. *Trends Biochem. Sci.*, **23**, 244–245.

Hiyama, H., Yokoi, M., Masutani, C., Sugasawa, K., Maekawa, T., Tanaka, K., Hoeijmakers, J.H. & Hanaoka, F. (1999) Interaction of hHR23 with S5a. The ubiquitin-like domain of hHR23 mediates interaction with S5a subunit of 26 S proteasome. *J. Biol. Chem.*, **274**, 28019–28025.

Hofmann, K. & Falquet, L. (2001) A ubiquitin-interacting motif conserved in components of the proteasomal and lysosomal protein degradation systems. *Trends Biochem. Sci.*, **26**, 347–350.

Imai, Y., Soda, M. & Takahashi, R. (2000) Parkin suppresses unfolded protein stress-induced cell death through its E3 ubiquitin-protein ligase activity. *J. Biol. Chem.*, **275**, 35661–35664.

Imai, Y., Soda, M., Inoue, H., Hattori, N., Mizuno, Y. & Takahashi, R. (2001) An unfolded putative transmembrane polypeptide, which can lead to endoplasmic reticulum stress, is a substrate of parkin. *Cell*, **105**, 891–902.

Jäger, S., Strayle, J., Heinemeyer, W. & Wolf, D.H. (2001) Cic1, an adaptor protein specifically linking the 26S proteasome to its substrate, the SCF component Cdc4. *EMBO J.*, **20**, 4423–4431.

Kawahara, H. *et al.* (2000) Developmentally regulated, alternative splicing of the Rpn10 gene generates multiple forms of 26S proteasomes. *EMBO J.*, **19**, 4144–4153.

Kikuchi, J., Iwahara, J., Kigawa, T., Murakami, Y., Okazaki, T. & Yokoyama, S. (2002) Solution structure determination of the two DNA-binding domains in the *Schizosaccharomyces pombe* abp1 protein by a combination of dipolar coupling and diffusion anisotropy restraints. *J. Biomol. NMR*, **22**, 333–347.

Kitada, T. *et al.* (1998) Mutations in the parkin gene cause autosomal recessive juvenile parkinsonism. *Nature*, **392**, 605–608.

Kleijnen, M.F., Shih, A.H., Zhou, P., Kumar, S., Soccio, R.E., Kedersha, N.L., Gill, G. & Howley, P.M. (2000) The hPLIC proteins may provide a link between the ubiquitination machinery and the proteasome. *Mol. Cell*, **6**, 409–419.

Koradi, R., Billeter, M. & Wüthrich, K. (1996) MOLMOL: A program for display and analysis of macromolecular structures. *J. Mol. Graph. Model.*, **14**, 51–55.

Lam, Y.A., Lawson, T.G., Velayutham, M., Zweier, J.L. & Pickart, C.M. (2002) A proteasomal ATPase subunit recognizes the polyubiquitin degradation signal. *Nature*, **416**, 763–767.

Laskowski, R.A., Rullmann, J.A., MacArthur, M.W., Kaptein, R. & Thornton, J.M. (1996) AQUA and PROCHECK-NMR: programs for checking the quality of protein structures solved by NMR. *J. Biomol. NMR*, **8**, 477–486.

Lücking, C.B. *et al.* (2000) Association between early-onset Parkinson's disease and mutations in the parkin gene. French Parkinson's Disease Genetics Study Group. *N. Engl. J. Med.*, **342**, 1560–1567.

Nilges, M., Gronenborn, A.M., Brünger, A.T. & Clore, G.M. (1988) Determination of three-dimensional structures of proteins by simulated annealing with interproton distance restraints. Application to crambin, potato carboxypeptidase inhibitor and barley serine proteinase inhibitor 2. *Protein Eng.*, **2**, 27–38.

Ottiger, M. & Bax, A. (1998) Characterization of magnetically oriented phospholipid micelles for measurement of dipolar couplings in macromolecules. *J. Biomol. NMR*, **12**, 261–372.

Saeki, Y., Sone, T., Toh-e, A. & Yokosawa, H. (2002) Identification of ubiquitin-like protein-binding subunits of the 26S proteasome. *Biochem. Biophys. Res. Commun.*, **296**, 813–819.

Shimura, H. *et al.* (2000) Familial Parkinson disease gene product, parkin, is a ubiquitin-protein ligase. *Nature Genet.*, **25**, 302–305.

Shimura, H. *et al.* (2001) Ubiquitination of a new form of alpha-synuclein by parkin from human brain: implications for Parkinson's disease. *Science*, **293**, 263–269.

Stein, E.G., Rice, L.M. & Brünger, A.T. (1997) Torsion-angle molecular dynamics as a new efficient tool for NMR structure calculation. *J. Magn. Reson.*, **124**, 154–164.

Terreni, L., Calabrese, E., Calella, A.M., Forloni, G. & Mariani, C. (2001) New mutation (R42P) of the parkin gene in the ubiquitinlike domain associated with parkinsonism. *Neurology*, **56**, 463–466.

Walters, K.J., Kleijnen, M.F., Goh, A.M., Wagner, G. & Howley, P.M. (2002) Structural studies of the interaction between ubiquitin family proteins and proteasome subunit S5a. *Biochemistry*, **41**, 1767–1777.

Wilkinson, C.R., Seeger, M., Hartmann-Petersen, R., Stone, M., Wallace, M., Semple, C. & Gordon, C. (2001) Proteins containing the UBA domain are able to bind to multi-ubiquitin chains. *Nature Cell Biol.*, **3**, 939–943.

Xie, Y. & Varshavsky, A. (2000) Physical association of ubiquitin ligase and the 26S proteasome. *Proc. Natl Acad. Sci. USA*, **97**, 2497–2502.

Yamamura, Y., Sobue, I., Ando, K., Iida, M. & Yanagi, T. (1973) Paralysis agitans of early onset with marked diurnal fluctuation of symptoms. *Neurology*, **23**, 239–244.

Young, P., Deveraux, Q., Beal, R.E., Pickart, C.M. & Rechsteiner, M. (1998) Characterization of two polyubiquitin binding sites in the 26 S protease subunit 5a. *J. Biol. Chem.*, **273**, 5461–5467.

Zhang, Y., Gao, J., Chung, K.K., Huang, H., Dawson, V.L. & Dawson, T.M. (2000) Parkin functions as an E2-dependent ubiquitin-protein ligase and promotes the degradation of the synaptic vesicle-associated protein, CDCrel-1. *Proc. Natl Acad. Sci. USA*, **97**, 13354–13359.

THE JOURNAL OF BIOLOGICAL CHEMISTRY
Vol. 278, No. 18, Issue of May 2, pp. 16237–16243, 2003
Printed in U.S.A.

Conditional Knockdown of Proteasomes Results in Cell-cycle Arrest and Enhanced Expression of Molecular Chaperones Hsp70 and Hsp40 in Chicken DT40 Cells*

Received for publication, February 6, 2003
Published, JBC Papers in Press, February 19, 2003, DOI 10.1074/jbc.M301331200

Tomoko Tanahashi-Hori‡, Nobuyuki Tanahashi§, Keiji Tanaka‡, and Tomoki Chiba‡¶

From the ‡Department of Molecular Oncology, The Tokyo Metropolitan Institute of Medical Science, 3-18-22 Honkomagome, Bunkyo-ku, Tokyo 113-8613 and the §EPM Project Groups, Osaka R&D Laboratories, Sumitomo Electric Industries Ltd., and New Energy and Industrial Technology Development Organization, Taya-cho 1, Sakae-ku, Yokohama 244-8588, Japan

The 26 S proteasome is an evolutionarily conserved ATP-dependent protease complex that degrades poly-ubiquitinated proteins and plays essential roles in a critical part of cellular regulation. In vertebrates, the roles of the proteasome have been widely studied by use of specific inhibitors, but not genetically. Here, we generated a cell line $Z^{-/-/-}$/Z-HA, in which the expression of the catalytic subunit of the proteasome, Z (β2) could be manipulated. This cell line expresses exogenous Z protein under the control of a tetracycline-repressible promoter in a Z-nullizygous genetic background. Treatment of these cells with doxycycline inhibited Z expression and, hence, the function of the proteasome. The latter resulted in accumulation of poly-ubiquitinated proteins and concomitant induction of molecular chaperones Hsp70 and Hsp40. These results suggest a synergistic role for the proteasome with these molecular chaperones to eliminate misfolded or damaged proteins *in vivo*. Furthermore, knockdown of the proteasome induced apoptotic cell death following cell-cycle arrest at G_2/M phase. Our $Z^{-/-/-}$/Z-HA cell line would be useful for evaluating proteolytic processes catalyzed by the proteasome in many biological events in vertebrate cells.

The 26 S proteasome with a molecular mass of ~2500 kDa consists of the central 20 S protease (catalytic core) and two outer 19 S regulatory particles (alias PA700), functioning as a protein-destroying machine responsible for energy-dependent proteolysis (1, 2). The 20 S proteasome is composed of two copies of 14 different subunits: 7 distinct α and 7 distinct β type subunits. It is a barrel-like particle formed by the axial stacking of four rings made up of two outer α-rings and inner β-rings, being associated in the order of αββα. Three out of seven β-type subunits of each inner ring have catalytically active threonine residues at their N termini, and these active sites reside in a chamber formed by the centers of the abutting β-rings. The eukaryotic 20 S proteasome has at least three different catalytic activities against synthetic peptide substrates; *i.e.* a trypsin-like, chymotrypsin-like, and caspase-like (or peptidylglutamyl-hydrolyzing) activities, that contribute to the hydrolysis of multiple peptide bonds in a single polypeptide by a coordinated mechanism (1, 3, 4).

To date, yeast proteasomal mutants and membrane-permeable inhibitors have been used to determine *in vivo* functions of proteasomes, which have created diverse arrays of evidence on the biological importance of proteasomes such as the cell cycle, immune response, signaling cascades, and protein quality control in various eukaryotes (5, 6). Indeed, budding yeast mutants that lack some peptidase activities have contributed greatly to our understanding of the involvement of proteasomes in the degradation of many unstable key proteins (7), but their application to higher organisms has not been tested. Various substrate-related peptidyl compounds such as MG-132 and $Z\text{-}L_3VS$ have been devised as potent inhibitors of proteasomes (8, 9), but caution must be exercised in their use for interpreting proteasome functions, because they inhibit not only proteasomes but also other proteases. In contrast to these compounds, new microbial metabolites, such as lactacystin and eponemycin, were found to induce selective inhibition of proteasomes that do not affect other proteases examined so far (10, 11). However, although these metabolites bind to active threonine residues of proteasomes, the possibility that they inhibit other as-yet-unidentified threonine protease(s) cannot be ruled out completely. Therefore, genetic approaches capable of manipulating proteasomal activities are still required to determine the *in vivo* functions of proteasomes in higher organisms such as vertebrate cells.

For this purpose, we disrupted proteasome subunit Z (formally designated β2) gene (*cpsmb7*) in chicken B cell line DT40 then established $Z^{-/-/-}$/Z-HA cells that express a tetracycline-repressible HA[1]-tagged Z protein (Z-HA). This construct could manipulate proteasome levels in vertebrate cells by repressing the Z-HA by doxycycline (Dox) treatment. Using these cells, we found that reduction of proteasomes caused not only G_2/M arrest during cell-cycle progression but also induction of apoptosis. Moreover, our results surprisingly showed that reduced proteasomes functions induced the expression of major molecular chaperones Hsp70 and Hsp40, suggesting a potential link

* This work was supported in part by a grant-in-aid from the Ministry of Education, Culture, Sports, Science and Technology, Japan. The costs of publication of this article were defrayed in part by the payment of page charges. This article must therefore be hereby marked "*advertisement*" in accordance with 18 U.S.C. Section 1734 solely to indicate this fact.

The nucleotide sequence(s) reported in this paper has been submitted to the GenBank™/EBI Data Bank with accession number(s) AB098728.

¶ To whom correspondence should be addressed. Tel./Fax: 81-3-3823-2237; E-mail: tchiba@rinshoken.or.jp.

[1] The abbreviations used are: HA, hemagglutinin; Bleo, phleomycin; Boc-LRR-AMC, *t*-butyloxycarbonyl-Leu-Arg-Arg-AMC; Bsd, blasticidin; Dox, doxycycline; ODC, ornithine decarboxylase; Puro, puromycin; Suc-LLVY-AMC, succinyl-Leu-Leu-Val-Tyr-7-amino-4-methycoumarine; tTA, tetracycline-controlled transactivator; Z-LLE-AMC, carbobenzoxy-Leu-Leu-Glu-AMC; TdT, terminal deoxytransferase; WST-8, 2-(2-methoxy-4-nitrophenyl)-3-(4-nitrophenyl)-5-(2,4-disulfophenyl)-2H-tetrazolium, monosodium salt; TUNEL, TdT-mediated dUTP-biotin nick end-labeling; ER, endoplasmic reticulum; UPR, unfolded protein response.

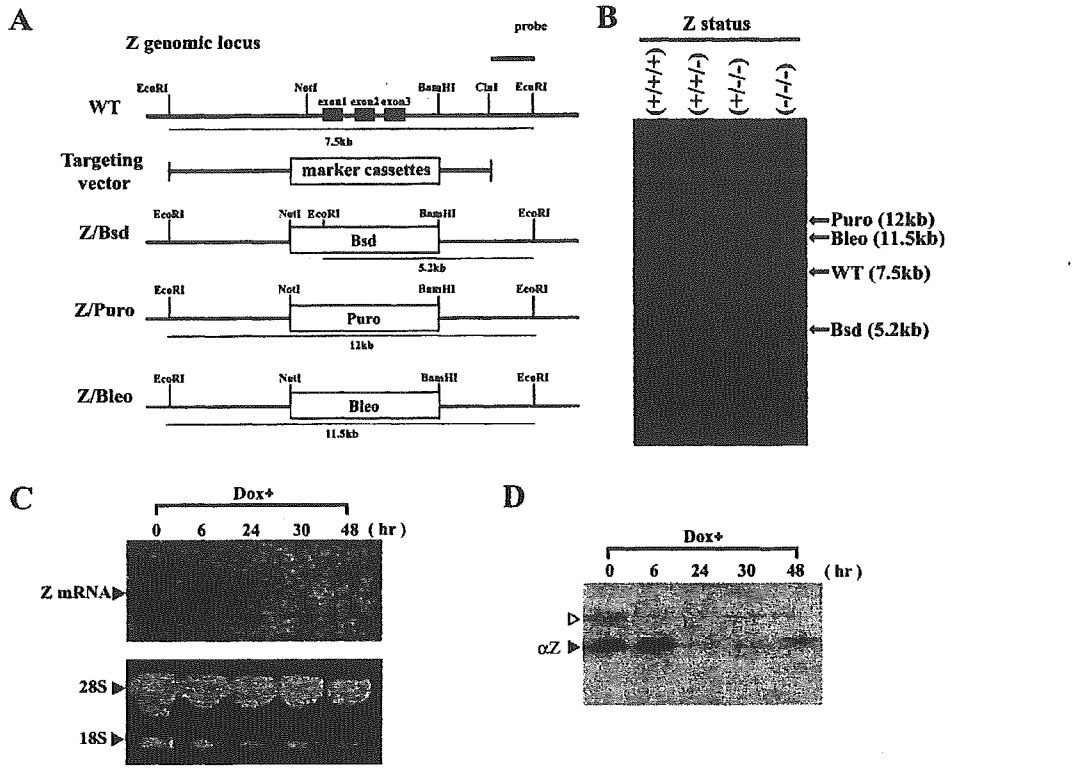

FIG. 1. **Conditional knockdown of proteasome Z subunit in DT40 cells.** *A*, schematic representation of part of Z locus and targeting vectors. Wild-type (*WT*) and targeted alleles (*Z/Bsd*, *Z/Puro*, and *Z/Bleo*) are shown. *B*, genomic Southern blot analysis of wild-type (+/+/+), two heterozygous mutants (+/+/− and +/−/−), and homozygous mutant (−/−/−). Genomic DNAs were digested with *Eco*RI and hybridized with the probe indicated in *A*. *C*, expression of Z-HA mRNA upon Dox treatment. $Z^{-/-/-}$/Z-HA cells were Dox-treated for the indicated times, and total RNAs were subjected to Northern blot analysis. Expression of Z-HA (*top*) and ethidium bromide staining of the total RNAs (*bottom*) are shown. *D*, expression of Z-HA protein upon Dox treatment. Cell extracts (2 μg of protein), obtained from cells treated as in *C*, were Western blotted with anti-chicken Z antibody. The *lower signal* is the mature form (*solid arrowhead*), whereas the *upper signal* corresponds to the precursor form (*open arrowhead*).

between proteasome-mediated proteolysis and stress response for protein homeostasis in the cell.

EXPERIMENTAL PROCEDURES

Plasmid Constructs—Partial chicken Z cDNA was obtained from DT40 cells-derived mRNAs by reverse transcription-PCR method. The primers (5′-GACACGAGGGCGACCGAAGGGATG-3′ and 5′-GCGGCT-GCTCAGGAAGTATCCATG-3′) were synthesized based on expressed sequence tag sequence (AJ397675). The full-length cDNA and genomic DNA were obtained by screening chicken muscle cDNA and genomic DNA libraries (Stratagene). The Z targeting vectors were designed by replacing the DNA segment that encompasses exon 1 to exon 3, with drug-resistant cassettes for blasticidin (Bsd), puromycin (Puro), and phleomycin (Bleo). A hemagglutinin (HA) tag was fused to the 3′-end of chicken Z cDNA coding regions by PCR amplifications. HA-tagged chicken Z cDNA (Z-HA) was inserted into the pUHD10–3 vector at the *Eco*RI site and the *Ssp*I site was replaced with the *Hin*dIII site by a *Hin*dIII linker. To construct a tetracycline (tet)-regulatable Z expression vector, tTA-dependent promoter flanked with HA-tagged chicken Z cDNA were recovered from pUHD10–3-Z-HA by digestion with *Hin*dIII and inserted into the *Hin*dIII site of ptTA2-Neo vector (Clontech) that encode tet-repressible tTA (tetR-VP16). The resulting plasmid (ptTA2-Neo-tetZ-HA) expresses Z-HA protein under the control of the tetR-VP16 (12).

Cell Culture and Transfection—DT40 cells were cultured in RPMI1640 medium containing 10% (v/v) fetal bovine serum, 5% (v/v) chicken serum, 10 μM 2-mercaptoethanol, and antibiotics (penicillin and streptomycin) at 39.5 °C under 5% CO_2. Cells were electroporated at 25 microfarads and 550 V (Bio-Rad) as described previously (13). Stable transformants were selected with each drug at the following concentrations: 2.0 mg/ml Geneticin (Sigma), 0.5 μg/ml puromycin (Sigma), 50 μg/ml blasticidin-S (Funakoshi), and 0.3 mg/ml phleomycin (Sigma). Cell viability was assayed by measuring the metabolic activity using tetrazolium salt WST-8 (2-(2-methoxy-4-nitrophenyl)-3-(4-nitrophenyl)-5-(2,4-disulfophenyl)-2H-tetrazolium, monosodium salt, Cell Counting Kit-8, Wako). After incubating the cells with WST-8, the optical density was read as specified by the manufacturer. Dox was used at a concentration of 2 μg/ml for the indicated times.

Antibodies—Anti-chicken Z polyclonal antibody was raised in rabbits using a purified recombinant His-tagged Z protein expressed in *Escherichia coli* BL21. Anti-Hsp70 (MBL), anti-Hsp40 (Stress Gen), anti-actin (Chemicon), anti-Wee1 (Santa Cruz Biotechnology), anti-poly-ubiquitin (MBL), horseradish peroxidase-conjugated anti-rabbit and anti-mouse IgG antibodies (Amersham Biosciences) were purchased.

Western Blot Analysis—Cells were lysed in 50 mM Tris-HCl (pH 8.0) containing 0.1% TritonX-100 and protease inhibitor mixture (Roche Molecular Biochemicals). Following a brief sonication, the extracts were cleared by centrifugation and subjected to 10–20% SDS-PAGE (14). After transfer onto polyvinylidene difluoride membranes (Millipore), proteins were detected by specific antibodies with the ECL method (Amersham Biosciences). Protein concentration was measured by the method of Bradford with bovine serum albumin as a standard (15).

Southern Blot Analysis—Genomic DNAs were isolated by using a DNeasy tissue kit (Qiagen). Genomic DNA (15 μg) was digested with *Eco*RI, separated in a 0.7% (w/v) agarose gel, and transferred onto a Hybond N^+ nylon membrane (Amersham Biosciences). The membrane was hybridized with ^{32}P-labeled probe (*Cla*I-*Eco*RI fragment indicated in Fig. 1A), washed at high stringency, and then autoradiographed.

Northern Blot Analysis—Total RNAs were isolated by using an RNeasy Mini kit (Qiagen). Approximately 15 μg of total RNAs was separated and transferred onto a Hybond N^+ nylon membrane. The membrane was hybridized with ^{32}P-labeled full-length chicken Z cDNA probe, washed at high stringency, and then autoradiographed.

Glycerol Gradient Fraction—Cells were lysed in 25 mM Tris-HCl (pH 7.5) containing 1 mM dithiothreitol with 2 mM ATP by sonication, and the lysates were centrifuged at 15,000 × *g* for 30 min. The supernatants were subjected to glycerol gradient centrifugation with 10–40% glycerol in the above buffer. After centrifugation at 83,000 × *g* for 22 h using a Beckman SW28 rotor, the gradient was separated into 30 fractions of 1 ml each (16).

Assay of Peptidase Activity—Hydrolysis of the synthetic peptides, succinyl-Leu-Leu-Val-Tyr-7-amino-4-methycoumarine (Suc-LLVY-AMC), *t*-butyloxycarbonyl-Leu-Arg-Arg-AMC (Boc-LRR-AMC), and carbobenzoxy-Leu-Leu-Glu-AMC (Z-LLE-AMC) was measured under the presence or absence of 0.05% SDS as described previously (17). One unit of peptidase activity was defined as the amount that degraded 1 nmol of a given fluorogenic peptide per minute.

Assay of [^{35}S]ODC Degradation Activity—^{35}S-Labeled ornithine decarboxylase (ODC) was produced *in vitro* by translating rat ODC mRNA in rabbit reticulocyte lysates with ^{35}S-labeled Met and Cys (PerkinElmer Life Sciences) and then immunopurified. The degradation of ODC was assayed as described previously (17). In brief, ^{35}S-labeled ODC (3000–4000 cpm) was incubated with antizyme, ATP, and enzyme solution in buffer containing the ATP regeneration system at 37 °C for 1 h. The reaction mixtures were then precipitated with trichloroacetic acid, the radioactivity of the trichloroacetic acid-soluble fraction was measured, and the activity was expressed as a percentage of total ODC radioactivity added.

Flow Cytometric Analysis—Cells were fixed in 70% ethanol in phosphate-buffered saline at 4 °C. Fixed cells were washed in phosphate-buffered saline, incubated with 0.25 mg/ml RNase A at 37 °C, and stained with 10 μg/ml propidium iodide at 4 °C. DNA contents were measured by a flow cytometry and cell cycle profiles were analyzed by the Expo ADC analysis program (Beckman Coulter).

Immunofluorescence and TUNEL Assay—Cells were fixed in 1% paraformaldehyde. For immunofluorescence analysis, anti-HA monoclonal antibody (BAbCO) and Alexa Fluor 594 goat anti-mouse IgG antibody (Molecular Probes) were used. Nuclei were counterstained with TOTO3 (Molecular Probes). Apoptotic cells were detected by TdT-mediated dUTP-biotin nick end-labeling (TUNEL) assay using an Apoptag kit (Intergen). The assay was performed according to instructions provided by the manufacturer. Fluorescence images were obtained using a confocal laser microscope (Zeiss and Bio-Rad).

RESULTS

Genetic Manipulation of Proteasome Function—To examine the cellular roles of proteasomes in vertebrates, we generated a cell line that could genetically manipulate the level of the proteasome subunit that confers a peptidase activity. Chicken B cell line DT40 is advantageous for this purpose, because of its efficient rate of homologous recombination (13). Full-length chicken Z cDNA was obtained by screening a chicken muscle cDNA library using the partial cDNA fragment obtained by reverse transcription-PCR. The full-length chicken Z cDNA deduced a protein of 277 amino acids (accession number AB098728), displaying 57.4% and 83.8% identities with *Saccharomyces cerevisiae* and human, respectively, at the amino acid level. To disrupt the proteasome Z gene (*cpsmb7*), chicken Z genomic DNA was isolated from chicken genomic DNA library, and the targeting vectors were constructed as shown in Fig. 1*A*. The vectors were designed to create a null allele by replacing the DNA segment that encompasses exon 1 to exon 3, which encodes the first 85 amino acids, including the essential catalytic site (threonine 44 in the exon 2), with drug-resistant cassettes. DT40 cells that contain three functional Z genes (*cpsmb7*) were successively transfected with each targeting vector, and the homologously recombined clones were identified by genomic Southern blot (Fig. 1*B*). Because the null mutant was expected to be lethal, we transfected the tet-regulatable Z-HA expression vector (ptTA2-Neo-tetZ-HA vector), in which the expression of Z protein could be shut off by Dox treatment, and isolated their stable transformants after the first allele was disrupted by Bsd construct. The second and third loci were disrupted by Puro and Bleo constructs, respectively. Finally, we obtained the $Z^{-/-/-}$/Z-HA clone that expressed Z-HA in a Z-nullizygous genetic background. The genomic Southern blots of representative clones are shown in Fig. 1*B*. Homologous recombination was identified as appearance of new 5.2-, 12-, and 11.5-kb bands corresponding to the targeted alleles generated by the Bsd, Puro, and Bleo constructs, respectively.

We then tested the effect of Dox treatment on Z-HA expression in $Z^{-/-/-}$/Z-HA cells. Dox treatment of $Z^{-/-/-}$/Z-HA cells reduced the mRNA and protein expression of Z-HA to undetectable levels at 24 h after Dox treatment (Fig. 1, *C* and *D*). Western blot with anti-Z antibody detected both precursor and mature forms of Z-HA. The latter form migrated below the size of the former (Fig. 1*D*). It is known that the catalytic subunits are synthesized as precursor forms and processed into the mature form during the assembly of the 20 S proteasome complex (18). The mature form co-sedimented with the 20 S proteasome, whereas the precursor form was detected in the lighter fraction when the cell extracts were fractionated by glycerol density gradient centrifugation (see Fig. 3, *lower panels*), suggesting that Z-HA is processed and incorporated into the 20 S proteasome.

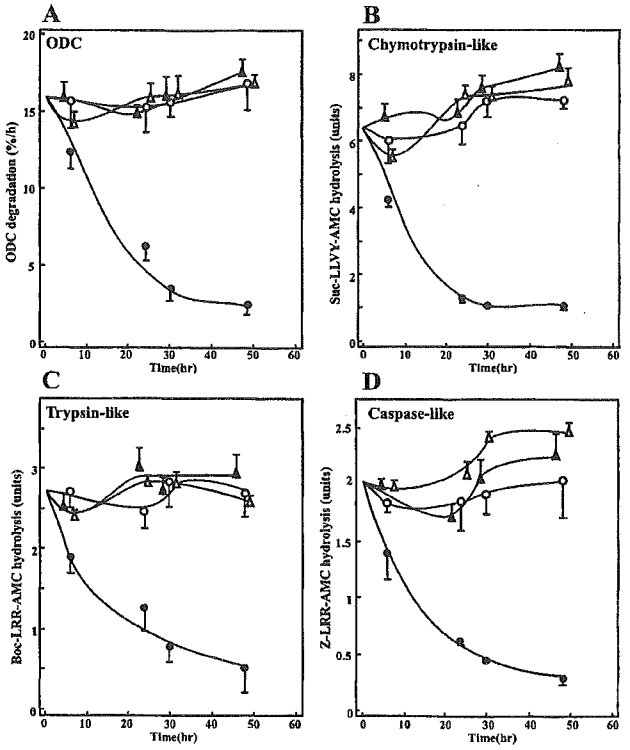

FIG. 2. **Proteasome activities in Dox-treated $Z^{-/-/-}$/Z-HA cells.** Cell extracts (20 μg of protein) were obtained from Dox-treated or untreated cells for indicated times, and peptidase activities were measured against ODC (*A*) and synthetic peptides; *i.e.* a chymotrypsin-like (*B*, Suc-LLVY-AMC), a trypsin-like (*C*, Boc-LRR-AMC), and a caspase-like (*D*, Z-LLE-AMC) activities. *Open circles*, Dox-untreated $Z^{-/-/-}$/Z-HA cells; *solid circles*, Dox-treated $Z^{-/-/-}$/Z-HA cells; *open triangles*, Dox-untreated wild-type cells; *solid triangles*, Dox-treated wild-type cells. Note that a caspase-like activity was assayed in the presence of 0.05% SDS, whereas the chymotrypsin-like and trypsin-like activities were without SDS (for the reason, see Fig. 3, *upper panels*, and text). Data represent the mean ± S.D. values of four independent analyses.

Depletion of Z Subunit Resulted in Loss of Proteasome Activity—Based on yeast studies, Pup1p, which corresponds to Z/β2, is known to confer trypsin-like activity (19, 20). In the next step, we tested whether loss of Z results in specific loss of trypsin-like activity. After Dox treatment, cells were serially collected at the indicated times and cell fractions were prepared. The cell fractions were first tested for their ability to degrade ODC, a proteasome-specific substrate independent of ubiquitination. As shown in Fig. 2*A*, ODC-degrading activities gradually decreased upon Dox treatment. These effects were not seen in Dox-untreated cells or Dox-treated wild-type DT40 cells. Testing for the specificity of peptidase activities showed that not only trypsin-like activity, but also other peptidase

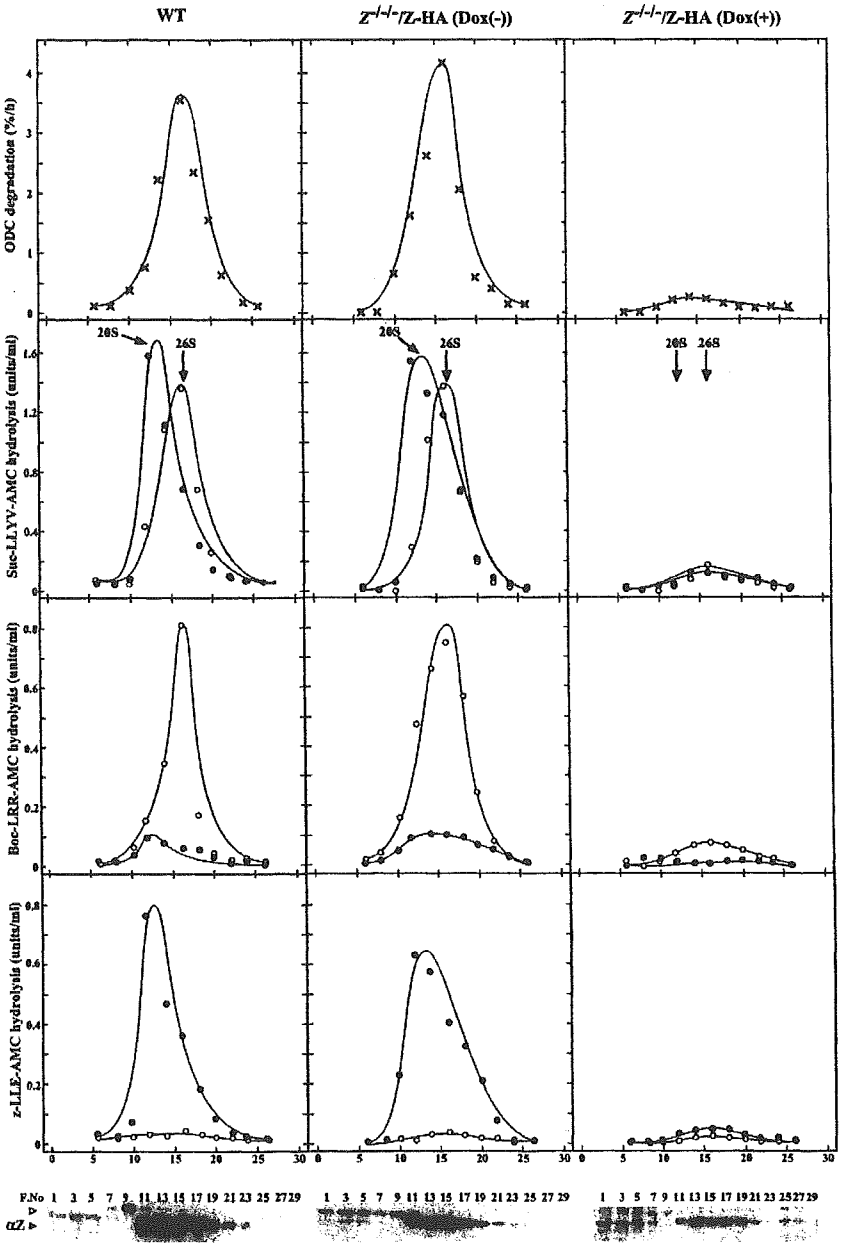

FIG. 3. **Sedimentation velocity analysis of wild-type and $Z^{-/-/-}$/Z-HA cell extracts.** Samples (4 mg of protein) of the wild-type (*WT*) and $Z^{-/-/-}$/Z-HA cells treated with or without Dox for 30 h were fractionated by glycerol density gradient centrifugation (10–40% glycerol from fractions 1 to 30) as described under "Experimental Procedures." After fractionation, aliquots (20 μl) of individual fractions were used for an assay of three peptide hydrolysis with (*solid circles*) or without (*open circles*) 0.05% SDS. The degradation of ^{35}S-ODC (*crosses*) was also assayed. Elution positions of purified 20 and 26 S proteasomes are shown. *Lower panel*, Western blot analysis. Proteins in 200 μl of each fraction were precipitated with acetone, subjected to SDS-PAGE, and stained by Western blot analysis using an anti-chicken Z antibody. *Numbers* correspond to fraction numbers in the *upper panels*. The *solid* and *open arrowheads* point to the mature and precursor forms of Z, respectively, similar to Fig. 1*D*.

chymotrypsin-like and caspase-like activities were reduced (Fig. 2, *B–D*).

To further confirm that these peptidase activities represent proteasome-specific activities, $Z^{-/-/-}$/Z-HA cells were treated with or without Dox for 30 h, and the cell extracts were further fractionated by glycerol density gradient centrifugation and subjected to peptidase assay and Western blot analysis. As shown in Fig. 3 (*upper panels*), in wild-type cells, active enzyme with chymotrypsin-like and trypsin-like activities was sedimented with a sedimentation coefficient of ~26 S, but low activity was found in slowly sedimenting fractions corresponding to the sedimentation position of the purified 20 S proteasome. Addition of 0.05% SDS, which is a potent artificial activator of the latent 20 S proteasome, caused marked enhancement of chymotrypsin-like activity in fractions sedimenting like the 20 S proteasome, as reported previously (16). Note that no obvious caspase-like activity was observed without SDS, but its strong activity could be measured in the presence of 0.05% SDS. ODC-degrading activity as well as these three types of peptidase activities were high and comparable in the Dox-untreated $Z^{-/-/-}$/Z-HA cells at wild-type levels, whereas they were greatly decreased in the Dox-treated $Z^{-/-/-}$/Z-HA cells (Fig. 3, *upper panels*).

Western blot analysis revealed that the mature form of Z protein migrated in the fractions 11–19 with 20–26 S proteasomes (Fig. 3, *lower panels*). The precursor form of Z in wild-type cell extracts migrated at lighter fractions 7–11. These fractions corresponded to 16 S pre-proteasomal particles as reported previously (18). On the other hand, the precursor Z-HA in Dox-untreated $Z^{-/-/-}$/Z-HA cell extracts was recovered in fractions 1–11. The precursor Z-HA observed in fractions 1–5 might be the free form based on its exogenous overexpression. Nonetheless, most mature Z-HA was recovered in the fractions containing sediments of 20–26 S proteasomes, indicating that Z-HA is assembled into these proteasomes. Of note, in the $Z^{-/-/-}$/Z-HA cells with Dox, the mature Z-HA was reduced, and